

COMPUTATIONAL HOMOGENISATION FOR NON-LINEAR HETEROGENEOUS SOLIDS

V. G. Kouznetsova^{*,†,‡}, M. G. D. Geers^{†,§} and W. A. M. Brekelmans^{†,¶}

**Netherlands Institute for Metals Research, Mekelweg 2
2628 CD Delft, The Netherlands*

*†Eindhoven University of Technology
Department of Mechanical Engineering, P. O. Box 513
5600 MB Eindhoven, The Netherlands*

‡V.G.Kouznetsova@tue.nl

§M.G.D.Geers@tue.nl

¶W.A.M.Brekelmans@tue.nl

This chapter presents a computational homogenisation strategy, which provides a rigorous approach to determine the macroscopic response of heterogeneous materials with accurate account for microstructural characteristics and evolution. When using this micro–macro strategy there is no necessity to define homogenised macroscopic constitutive equations, which, in the case of large deformations and complex microstructures, would be generally a hardly feasible task. Instead, the constitutive behaviour at macroscopic integration points is determined by averaging the response of the deforming microstructure. This enables a straightforward application of the method to geometrically and physically non-linear problems, making it a particularly valuable tool for the modelling of evolving non-linear heterogeneous microstructures under complex macroscopic loading paths. In this chapter, the underlying concepts and the details of the computational homogenisation technique are given. Formulation of the microscopic boundary value problem and the consistent micro–macro coupling in a geometrically and physically non-linear framework are elaborated. The implementation of the computational homogenisation scheme in a finite element framework is discussed. Some recent extensions of the computational homogenisation schemes are summarised.

1. Introduction

Industrial and engineering materials, as well as natural materials, are heterogeneous at a certain scale. Typical examples include metal alloy systems, polycrystalline materials, composites, polymer blends, porous and cracked media, biological materials and many functional materials. This

heterogeneous nature has a significant impact on the observed macroscopic behaviour of multiphase materials. Various phenomena occurring on the macroscopic level originate from the physics and mechanics of the underlying microstructure. The overall behaviour of micro-heterogeneous materials depends strongly on the size, shape, spatial distribution and properties of the microstructural constituents and their respective interfaces. The microstructural morphology and properties may also evolve under a macroscopic thermo-mechanical loading. Consequently, these microstructural influences are important for the processing and the reliability of the material and resulting products.

Determination of the macroscopic overall characteristics of heterogeneous media is an essential problem in many engineering applications. Studying the relation between microstructural phenomena and the macroscopic behaviour not only allows to predict the behaviour of existing multiphase materials, but also provides a tool to design a material microstructure such that the resulting macroscopic behaviour exhibits the required characteristics. An additional challenge for multiscale modelling is provided by ongoing technological developments, e.g. miniaturisation of products, development of functional and smart materials and increasing complexity of forming operations. In micro and submicron applications the microstructure is no longer negligible with respect to the component size, thus giving rise to a so-called size effect. Functional materials (e.g. as used in flexible electronics) typically involve materials with large thermo-mechanical mismatches combined with highly complex interconnects. Furthermore, advanced forming operations force a material to undergo complex loading paths. This results in varying microstructural responses and easily provokes an evolution of the microstructure, e.g. phase transformations. From an economical (time and costs) point of view, performing straightforward experimental measurements on a number of material samples of different sizes, accounting for various geometrical and physical phase properties, volume fractions and loading paths is a hardly feasible task. Hence, there is a clear need for modelling strategies that provide a better understanding of micro–macro structure–property relations in multiphase materials.

The simplest method leading to homogenised moduli of a heterogeneous material is based on the rule of mixtures. The overall property is then calculated as an average over the respective properties of the constituents, weighted with their volume fractions. This approach takes only one microstructural characteristic, i.e. the volume ratio of the heterogeneities,

into consideration and, strictly speaking, denies the influence of other aspects.

A more sophisticated method is the effective medium approximation, as established by Eshelby¹ and further developed by a number of authors.²⁻⁴ Equivalent material properties are derived as a result of the analytical (or semi-analytical) solution of a boundary value problem (BVP) for a spherical or ellipsoidal inclusion of one material in an infinite matrix of another material. An extension of this method is the self-consistent approach, in which a particle of one phase is embedded into an effective material, the properties of which are not known *a priori*.^{5,6} These strategies give a reasonable approximation for structures that possess some kind of geometrical regularity, but fail to describe the behaviour of clustered structures. Moreover, high contrasts between the properties of the phases cannot be represented accurately.

Although some work has been done on the extension of the self-consistent approach to non-linear cases (originating from the work by Hill⁵ who has proposed an “incremental” version of the self-consistent method), significantly more progress in estimating advanced properties of composites has been achieved by variational bounding methods.⁷⁻¹⁰ The variational bounding methods are based on suitable variational (minimum energy) principles and provide upper and lower bounds for the overall composite properties.

Another homogenisation approach is based on the mathematical asymptotic homogenisation theory.^{11,12} This method applies an asymptotic expansion of displacement and stress fields on a “natural scale parameter”, which is the ratio of a characteristic size of the heterogeneities and a measure of the macrostructure.¹³⁻¹⁷ The asymptotic homogenisation approach provides effective overall properties as well as local stress and strain values. However, usually the considerations are restricted to very simple microscopic geometries and simple material models, mostly at small strains. A comprehensive overview of different homogenisation methods may be found in a work done by Nemat-Nasser and Hori.¹⁸

The increasing complexity of microstructural mechanical and physical behaviour, along with the development of computational methods, made the class of so-called unit cell methods attractive. These approaches have been used in a great number of different applications.¹⁹⁻²⁶ A selection of examples in the field of metal matrix composites has been collected, for example, in a work done by Suresh *et al.*²⁷ The unit cell methods serve a twofold purpose: they provide valuable information on the local microstructural

fields as well as the effective material properties. These properties are generally determined by fitting the averaged microscopical stress–strain fields, resulting from the analysis of a microstructural representative cell subjected to a certain loading path, on macroscopic closed-form phenomenological constitutive equations in a format established *a priori*. Once the constitutive behaviour becomes non-linear (geometrically, physically or both), it becomes intrinsically difficult to make a well-motivated assumption on a suitable macroscopic constitutive format. For example, McHugh *et al.*²⁸ have demonstrated that when a composite is characterised by power-law slip system hardening, the power-law hardening behaviour is not preserved at the macroscale. Hence, most of the known homogenisation techniques are not suitable for large deformations nor complex loading paths, neither do they account for the geometrical and physical changes of the microstructure (which is relevant, for example, when dealing with phase transitions).

In recent years, a promising alternative approach for the homogenisation of engineering materials has been developed, i.e. multiscale computational homogenisation, also called global–local analysis or FE² in a more particular form. Computational homogenisation is a multiscale technique, which is essentially based on the derivation of the local macroscopic constitutive response (input leading to output, e.g. stress driven by deformation) from the underlying microstructure through the adequate construction and solution of a microstructural BVP.

The basic principles of the classical computational homogenisation have gradually evolved from concepts employed in other homogenisation methods and may be fit into the four-step homogenisation scheme established by Suquet²⁹: (i) definition of a microstructural representative volume element (RVE), of which the constitutive behaviour of individual constituents is assumed to be known; (ii) formulation of the microscopic boundary conditions from the macroscopic input variables and their application on the RVE (macro-to-micro transition); (iii) calculation of the macroscopic output variables from the analysis of the deformed microstructural RVE (micro-to-macro transition); (iv) obtaining the (numerical) relation between the macroscopic input and output variables. The main ideas of the computational homogenisation have been established by Suquet²⁹ and Guedes and Kikuchi¹⁵ and further developed and improved in more recent works.^{30–42}

Among several advantageous characteristics of the computational homogenisation technique the following are worth to be mentioned.

Techniques of this type

- do not require any explicit assumptions on the format of the macroscopic local constitutive equations, since the macroscopic constitutive behaviour is obtained from the solution of the associated microscale BVP;
- enable the incorporation of large deformations and rotations on both micro- and macrolevels;
- are suitable for arbitrary material behaviour, including physically non-linear and time dependent;
- provide the possibility to introduce detailed microstructural information, including the physical and geometrical evolution of the microstructure, into the macroscopic analysis;
- allow the use of any modelling technique on the microlevel, e.g. the finite element method (FEM),^{33,37,38,40} the boundary element method,⁴³ the Voronoi cell method,^{31,32} a crystal plasticity framework^{34,35} or numerical methods based on Fast Fourier Transforms^{36,44} and Transformation Field Analysis.⁴⁵

Although the fully coupled micro–macro technique (i.e. the solution of a nested BVP) is still computationally rather expensive, this concern can be overcome by naturally parallelising computations.^{37,42} Another option is selective usage, where non-critical regions are modelled by continuum closed-form homogenised constitutive relations or by the constitutive tangents obtained from the microstructural analysis but kept constant in the elastic domain, while in the critical regions the multiscale analysis of the microstructure is fully performed.³⁹ Despite the required computational efforts the computational homogenisation technique has proven to be a valuable tool to establish non-linear micro–macro structure–property relations, especially in the cases where the complexity of the mechanical and geometrical microstructural properties and the evolving character prohibit the use of other homogenisation methods. Moreover, this direct micro–macro modelling technique is useful for constructing, evaluating and verifying other homogenisation methods or micromechanically based macroscopic constitutive models.

In this chapter a computational homogenisation scheme is presented and details of its numerical implementation are elaborated. After a short summary of the underlying hypotheses and general framework of the computational homogenisation in Sec. 2, the microstructural BVP is stated and different types of boundary conditions are discussed in Sec. 3. Section 4 summarises the averaging theorems providing the basis for the

micro–macro coupling. Several types of boundary conditions are shown to automatically satisfy these theorems. Next, in Sec. 5, implementation issues are discussed, whereby special attention is given to the imposition of the periodic boundary conditions and extraction of the overall stress tensor and the consistent tangent operator. The coupled nested solution scheme is summarised in Sec. 6 followed by a simple illustrative example. A general concept of an RVE in the computational homogenisation context is discussed in Sec. 8. Finally, in Sec. 9 several extensions of the classical computational homogenisation scheme are outlined, i.e. homogenisation towards second gradient continuum, computational homogenisation for beams and shells and computational homogenisation for heat conduction problems.

Cartesian tensors and tensor products are used throughout the chapter: \mathbf{a} , \mathbf{A} and ${}^n\mathbf{A}$ denote, respectively, a vector, a second-order tensor and a n th-order tensor, respectively. The following notation for vector and tensor operations is employed: the dyadic product $\mathbf{ab} = a_i b_j \mathbf{e}_i \mathbf{e}_j$ and the scalar products $\mathbf{A} \cdot \mathbf{B} = A_{ij} B_{jk} \mathbf{e}_i \mathbf{e}_k$, $\mathbf{A} : \mathbf{B} = A_{ij} B_{ji}$, with $\mathbf{e}_i, i = 1, 2, 3$ the unit vectors of a Cartesian basis; conjugation $A_{ij}^c = A_{ji}$. A matrix and a column are denoted by $\underline{\mathbf{A}}$ and \underline{a} , respectively. The subscript “M” refers to a macroscopic quantity, whereas the subscript “m” denotes a microscopic quantity.

2. Basic Hypotheses

The material configuration to be considered is assumed to be macroscopically sufficiently homogeneous, but microscopically heterogeneous (the morphology consists of distinguishable components as, e.g. inclusions, grains, interfaces, cavities). This is schematically illustrated in Fig. 1. The

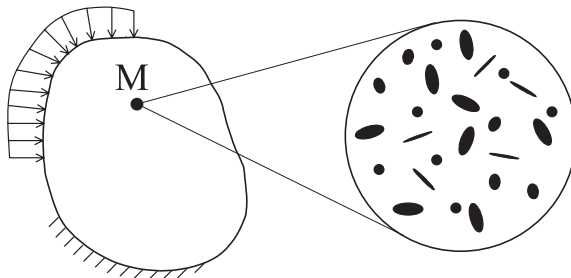


Fig. 1. Continuum macrostructure and heterogeneous microstructure associated with the macroscopic point M.

microscopic length scale is much larger than the molecular dimensions, so that a continuum approach is justified for every constituent. At the same time, in the context of the principle of separation of scales, the microscopic length scale should be much smaller than the characteristic size of the microscopic sample or the wave length of the macroscopic loading.

Most of the homogenisation approaches make an assumption on global periodicity of the microstructure, suggesting that the whole macroscopic specimen consists of spatially repeated unit cells. In the computational homogenisation approach, a more realistic assumption on local periodicity is proposed, i.e. the microstructure can have different morphologies corresponding to different macroscopic points, while it repeats itself in a small vicinity of each individual macroscopic point. The concept of local and global periodicity is schematically illustrated in Fig. 2. The assumption of local periodicity adopted in the computational homogenisation allows the modelling of the effects of a non-uniform distribution of the microstructure on the macroscopic response (e.g. in functionally graded materials).

In the classical computational homogenisation procedure, a macroscopic deformation (gradient) tensor \mathbf{F}_M is calculated for every material point of the macrostructure (e.g. the integration points of the macroscopic mesh within a finite element (FE) environment). The deformation tensor \mathbf{F}_M for a macroscopic point is next used to formulate the boundary conditions to be imposed on the RVE that is assigned to this point. Upon the solution of the BVP for the RVE, the macroscopic stress tensor \mathbf{P}_M is obtained by averaging the resulting RVE stress field over the volume of the RVE. As a

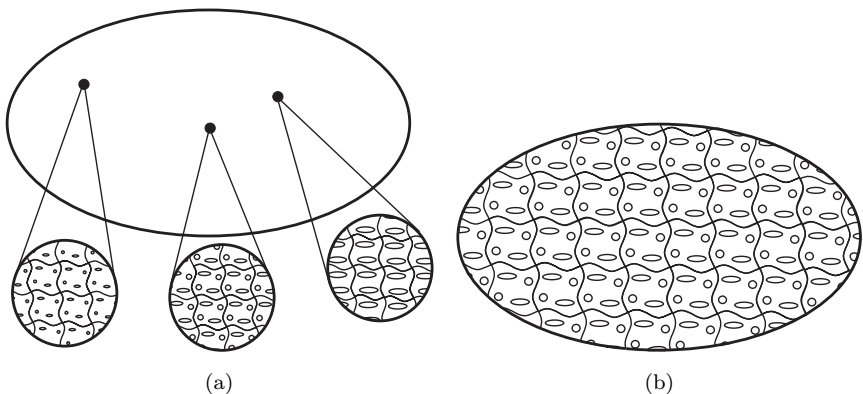


Fig. 2. Schematic representation of a macrostructure with (a) a locally and (b) a globally periodic microstructure.

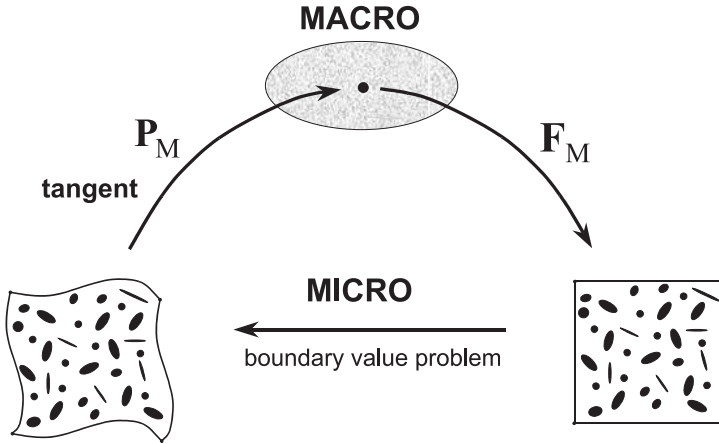


Fig. 3. Computational homogenisation scheme.

result, the (numerical) stress–deformation relationship at the macroscopic point is readily available. Additionally, the local macroscopic consistent tangent is derived from the microstructural stiffness. This framework is schematically illustrated in Fig. 3. This computational homogenisation technique is built entirely within a standard local continuum mechanics concept, where the response at a (macroscopic) material point depends only on the first gradient of the displacement field. Thus, this computational homogenisation framework is sometimes referred to as the “first-order”.

The micro–macro procedure outlined here is “deformation driven”, i.e. on the local macroscopic level the problem is formulated as follows: given a macroscopic deformation gradient tensor \mathbf{F}_M , determine the stress \mathbf{P}_M and the constitutive tangent, based on the response of the underlying microstructure. A “stress-driven” procedure (given a local macroscopic stress, obtain the deformation) is also possible. However, such a procedure does not directly fit into the standard displacement-based FE framework, which is usually employed for the solution of macroscopic BVPs. Moreover, in the case of large deformations, the macroscopic rotational effects have to be added to the stress tensor in order to uniquely determine the deformation gradient tensor, thus complicating the implementation. Therefore, the “stress-driven” approach, which is often used in the analysis of single unit cells, is generally not adopted in coupled micro–macro computational homogenisation strategies.

In the subsequent sections, the essential steps of the first-order computational homogenisation process are discussed in more detail. First the problem on the microlevel is defined, then the aspects of the coupling between micro- and macrolevel are considered and finally the realisation of the whole procedure within an FE context is explained.

3. Definition of the Problem on the Microlevel

The physical and geometrical properties of the microstructure are identified by an RVE. An example of a typical two-dimensional RVE is depicted in Fig. 4. The actual choice of the RVE is a rather delicate task. The RVE should be large enough to represent the microstructure, without introducing non-existing properties (e.g. undesired anisotropy) and at the same time it should be small enough to allow efficient computational modelling. Some issues related to the concept of a representative cell are discussed in Sec. 8. Here it is supposed that an appropriate RVE has been already selected. Then the problem on the RVE level can be formulated as a standard problem in quasi-static continuum solid mechanics.

The RVE deformation field in a point with the initial position vector \mathbf{X} (in the reference domain V_0) and the actual position vector \mathbf{x} (in the current domain V) is described by the microstructural deformation gradient tensor $\mathbf{F}_m = (\nabla_{0m}\mathbf{x})^c$, where the gradient operator ∇_{0m} is taken with respect to the reference microstructural configuration.

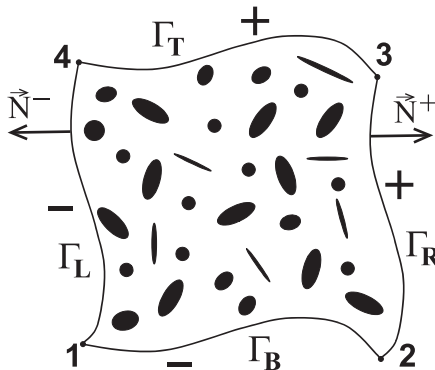


Fig. 4. Schematic representation of a typical two-dimensional representative volume element (RVE).

The RVE is in a state of equilibrium. This is mathematically reflected by the equilibrium equation in terms of the Cauchy stress tensor $\boldsymbol{\sigma}_m$ or, alternatively, in terms of the first Piola–Kirchhoff stress tensor $\mathbf{P}_m = \det(\mathbf{F}_m)\boldsymbol{\sigma}_m \cdot (\mathbf{F}_m^c)^{-1}$ according to (in the absence of body forces)

$$\nabla_m \cdot \boldsymbol{\sigma}_m = \mathbf{0} \text{ in } V \quad \text{or} \quad \nabla_{0m} \cdot \mathbf{P}_m^c = \mathbf{0} \text{ in } V_0, \quad (1)$$

where ∇_m is the the gradient operator with respect to the current configuration of the microstructural cell.

The mechanical characterisations of the microstructural components are described by certain constitutive laws, specifying a time- and history-dependent stress–deformation relationship for every microstructural constituent

$$\begin{aligned} \boldsymbol{\sigma}_m^{(\alpha)}(t) &= \mathcal{F}_\sigma^{(\alpha)}\{\mathbf{F}_m^{(\alpha)}(\tau), \tau \in [0, t]\} \quad \text{or} \\ \mathbf{P}_m^{(\alpha)}(t) &= \mathcal{F}_P^{(\alpha)}\{\mathbf{F}_m^{(\alpha)}(\tau), \tau \in [0, t]\}, \end{aligned} \quad (2)$$

where t denotes the current time; $\alpha = \overline{1, N}$, with N being the number of microstructural constituents to be distinguished (e.g. matrix, inclusion, etc.).

The actual macro-to-micro transition is performed by imposing the macroscopic deformation gradient tensor \mathbf{F}_M on the microstructural RVE through a specific approach. Probably the simplest way is to assume that all the microstructural constituents undergo a constant deformation identical to the macroscopic one. In the literature this is called the Taylor (or Voigt) assumption. Another simple strategy is to assume an identical constant stress (and additionally identical rotation) in all the components. This is called the Sachs (or Reuss) assumption. Also some intermediate procedures are possible, where the Taylor and Sachs assumptions are applied only to certain components of the deformation and stress tensors. All these simplified procedures do not really require a detailed microstructural modelling. Accordingly, they generally provide very rough estimates of the overall material properties and are hardly suitable in the non-linear deformation regimes. The Taylor assumption usually overestimates the overall stiffness, whereas the Sachs assumption leads to an underestimation of the stiffness. Nevertheless, the Taylor and Sachs averaging procedures are sometimes used to quickly obtain a first estimate of the composite’s overall stiffness. The Taylor assumption and some intermediate procedures are often employed in polycrystal plasticity modelling.

More accurate averaging strategies that do require the solution of the detailed microstructural BVP transfer the given macroscopic variables to the microstructural RVE via the boundary conditions. Classically three

types of RVE boundary conditions are used, i.e. prescribed displacements, prescribed tractions and prescribed periodicity.

In the case of prescribed displacement boundary conditions, the position vector of a point on the RVE boundary in the deformed state is given by

$$\mathbf{x} = \mathbf{F}_M \cdot \mathbf{X} \quad \text{with } \mathbf{X} \text{ on } \Gamma_0, \quad (3)$$

where Γ_0 denotes the undeformed boundary of the RVE. This condition prescribes a linear mapping of the RVE boundary.

For the traction boundary conditions, it is prescribed

$$\mathbf{t} = \mathbf{n} \cdot \boldsymbol{\sigma}_M \text{ on } \Gamma \quad \text{or} \quad \mathbf{p} = \mathbf{N} \cdot \mathbf{P}_M^c \text{ on } \Gamma_0, \quad (4)$$

where \mathbf{n} and \mathbf{N} are the normals to the current (Γ) and initial (Γ_0) RVE boundaries, respectively. However, the traction boundary conditions (4) do not completely define the microstructural BVP, as discussed at the end of Sec. 2. Moreover, they are not appropriate in the deformation driven procedure to be pursued in the present computational homogenisation scheme. Therefore, the RVE traction boundary conditions are not used in the actual implementation of the coupled computational homogenisation scheme; they were presented here for the sake of generality only.

Based on the assumption of microstructural periodicity presented in Sec. 2, periodic boundary conditions are introduced. The periodicity conditions for the microstructural RVE are written in a general format as

$$\mathbf{x}^+ - \mathbf{x}^- = \mathbf{F}_M \cdot (\mathbf{X}^+ - \mathbf{X}^-), \quad (5)$$

$$\mathbf{p}^+ = -\mathbf{p}^-, \quad (6)$$

representing periodic deformations (5) and antiperiodic tractions (6) on the boundary of the RVE. Here the (opposite) parts of the RVE boundary Γ_0^- and Γ_0^+ are defined such that $\mathbf{N}^- = -\mathbf{N}^+$ at corresponding points on Γ_0^- and Γ_0^+ , see Fig. 4. The periodicity condition (5), being prescribed on an initially periodic RVE, preserves the periodicity of the RVE in the deformed state. Also it should be mentioned that, as has been observed by several authors,^{46,47} the periodic boundary conditions provide a better estimation of the overall properties than the prescribed displacement or prescribed traction boundary conditions (see also the discussion in Sec. 8).

Other types of RVE boundary conditions are possible. The only general requirement is that they should be consistent with the so-called averaging theorems. The averaging theorems, dealing with the coupling between the micro- and macrolevels in an energetically consistent way, will be presented in the following section. The consistency of the three types of boundary conditions presented above with these averaging theorems will be verified.

4. Coupling of the Macroscopic and Microscopic Levels

The actual coupling between the macroscopic and microscopic levels is based on averaging theorems. The integral averaging expressions have been initially proposed by Hill⁴⁸ for small deformations and later extended to a large deformation framework.^{49,50}

4.1. Deformation

The first of the averaging relations concerns the micro–macro coupling of kinematic quantities. It is postulated that the macroscopic deformation gradient tensor \mathbf{F}_M is the volume average of the microstructural deformation gradient tensor \mathbf{F}_m

$$\mathbf{F}_M = \frac{1}{V_0} \int_{V_0} \mathbf{F}_m dV_0 = \frac{1}{V_0} \int_{\Gamma_0} \mathbf{x} \mathbf{N} d\Gamma_0, \quad (7)$$

where the divergence theorem has been used to transform the integral over the undeformed volume V_0 of the RVE to a surface integral.

Verification that the use of the prescribed displacement boundary conditions (3) indeed leads to satisfaction of (7) is rather trivial. Substitution of (3) into (7) and use of the divergence theorem with account for $\nabla_{0m} \mathbf{X} = \mathbf{I}$ give

$$\begin{aligned} \mathbf{F}_M &= \frac{1}{V_0} \int_{\Gamma_0} (\mathbf{F}_M \cdot \mathbf{X}) \mathbf{N} d\Gamma_0 \\ &= \frac{1}{V_0} \mathbf{F}_M \cdot \int_{\Gamma_0} \mathbf{X} \mathbf{N} d\Gamma_0 = \frac{1}{V_0} \mathbf{F}_M \cdot \int_{V_0} (\nabla_{0m} \mathbf{X})^c dV_0 = \mathbf{F}_M. \end{aligned} \quad (8)$$

The validation for the periodic boundary conditions (5) follows the same lines except that the RVE boundary is split into the parts Γ_0^+ and Γ_0^-

$$\begin{aligned} \mathbf{F}_M &= \frac{1}{V_0} \left\{ \int_{\Gamma_0^+} \mathbf{x}^+ \mathbf{N}^+ d\Gamma_0 + \int_{\Gamma_0^-} \mathbf{x}^- \mathbf{N}^- d\Gamma_0 \right\} \\ &= \frac{1}{V_0} \int_{\Gamma_0^+} (\mathbf{x}^+ - \mathbf{x}^-) \mathbf{N}^+ d\Gamma_0 \\ &= \frac{1}{V_0} \mathbf{F}_M \cdot \int_{\Gamma_0^+} (\mathbf{X}^+ - \mathbf{X}^-) \mathbf{N}^+ d\Gamma_0 = \frac{1}{V_0} \mathbf{F}_M \cdot \int_{\Gamma_0} \mathbf{X} \mathbf{N} d\Gamma_0 = \mathbf{F}_M. \end{aligned} \quad (9)$$

In the general case of large strains and large rotations, attention should be given to the fact that due to the non-linear character of the relations between different kinematic measures not all macroscopic kinematic quantities may be obtained as the volume average of their microstructural counterparts. For example, the volume average of the Green–Lagrange strain tensor

$$\mathbf{E}_M^* = \frac{1}{2V_0} \int_{V_0} (\mathbf{F}_m^c \cdot \mathbf{F}_m - \mathbf{I}) dV_0 \quad (10)$$

is in general not equal to the macroscopic Green–Lagrange strain obtained according to

$$\mathbf{E}_M = \frac{1}{2} (\mathbf{F}_M^c \cdot \mathbf{F}_M - \mathbf{I}). \quad (11)$$

4.2. Stress

Similarly, the averaging relation for the first Piola–Kirchhoff stress tensor is established as

$$\mathbf{P}_M = \frac{1}{V_0} \int_{V_0} \mathbf{P}_m dV_0. \quad (12)$$

In order to express the macroscopic first Piola–Kirchhoff stress tensor \mathbf{P}_M in the microstructural quantities defined on the RVE surface, the following relation is used (with account for microscopic equilibrium $\nabla_{0m} \cdot \mathbf{P}_m^c = \mathbf{0}$ and the equality $\nabla_{0m} \mathbf{X} = \mathbf{I}$):

$$\mathbf{P}_m = (\nabla_{0m} \cdot \mathbf{P}_m^c) \mathbf{X} + \mathbf{P}_m \cdot (\nabla_{0m} \mathbf{X}) = \nabla_{0m} \cdot (\mathbf{P}_m^c \mathbf{X}). \quad (13)$$

Substitution of (13) into (12), application of the divergence theorem, and the definition of the first Piola–Kirchhoff stress vector $\mathbf{p} = \mathbf{N} \cdot \mathbf{P}_m^c$ give

$$\mathbf{P}_M = \frac{1}{V_0} \int_{V_0} \nabla_{0m} \cdot (\mathbf{P}_m^c \mathbf{X}) dV_0 = \frac{1}{V_0} \int_{\Gamma_0} \mathbf{N} \cdot \mathbf{P}_m^c \mathbf{X} d\Gamma_0 = \frac{1}{V_0} \int_{\Gamma_0} \mathbf{p} \mathbf{X} d\Gamma_0. \quad (14)$$

Now it is a trivial task to validate that substitution of the traction boundary conditions (4₂) into this equation leads to an identity.

The volume average of the microscopic Cauchy stress tensor $\boldsymbol{\sigma}_m$ over the current RVE volume V can be elaborated similarly to (14)

$$\boldsymbol{\sigma}_M^* = \frac{1}{V} \int_V \boldsymbol{\sigma}_m dV = \frac{1}{V} \int_{\Gamma} \mathbf{t} \mathbf{x} d\Gamma. \quad (15)$$

Just as it is the case for kinematic quantities, the usual continuum mechanics relation between stress measures (e.g. the Cauchy and the first Piola–Kirchhoff stress tensors) is, in general, not valid for the volume averages of the microstructural counterparts $\boldsymbol{\sigma}_M^* \neq \mathbf{P}_M \cdot \mathbf{F}_M^c / \det(\mathbf{F}_M)$. However, the Cauchy stress tensor on the macrolevel should be defined as

$$\boldsymbol{\sigma}_M = \frac{1}{\det(\mathbf{F}_M)} \mathbf{P}_M \cdot \mathbf{F}_M^c. \quad (16)$$

Clearly, there is some arbitrariness in the choice of associated deformation and stress quantities, whose macroscopic measures are obtained as a volume average of their microscopic counterparts. The remaining macroscopic measures are then expressed in terms of these averaged quantities using the standard continuum mechanics relations. The specific selection should be made with care and based on experimental results and convenience of the implementation. The actual choice of the “primary” averaging measures: the deformation gradient tensor \mathbf{F} and the first Piola–Kirchhoff stress tensor \mathbf{P} (and their rates) has been advocated in the literature^{34,49,50} (in the last two references the nominal stress $\mathbf{S}_N = \det(\mathbf{F})\mathbf{F}^{-1} \cdot \boldsymbol{\sigma} = \mathbf{P}^c$ has been used). This particular choice is motivated by the fact that these two measures are work conjugated, combined with the observation that their volume averages can exclusively be defined in terms of the microstructural quantities on the RVE boundary only. This feature will be used in the following section, where the averaging theorem for the micro–macro energy transition is discussed.

4.3. Internal work

The energy averaging theorem, known in the literature as the Hill–Mandel condition or macrohomogeneity condition,^{29,48} requires that the macroscopic volume average of the variation of work performed on the RVE is equal to the local variation of the work on the macroscale. Formulated in terms of a work conjugated set, i.e. the deformation gradient tensor and the first Piola–Kirchhoff stress tensor, the Hill–Mandel condition reads

$$\frac{1}{V_0} \int_{V_0} \mathbf{P}_m : \delta \mathbf{F}_m^c \, dV_0 = \mathbf{P}_M : \delta \mathbf{F}_M^c \quad \forall \delta \mathbf{x}. \quad (17)$$

The averaged microstructural work in the left-hand side of (17) may be expressed in terms of RVE surface quantities

$$\delta W_{0M} = \frac{1}{V_0} \int_{V_0} \mathbf{P}_m : \delta \mathbf{F}_m^c dV_0 = \frac{1}{V_0} \int_{\Gamma_0} \mathbf{p} \cdot \delta \mathbf{x} d\Gamma_0, \quad (18)$$

where the relation (with account for microstructural equilibrium)

$$\mathbf{P}_m : \nabla_{0m} \delta \mathbf{x} = \nabla_{0m} \cdot (\mathbf{P}_m^c \cdot \delta \mathbf{x}) - (\nabla_{0m} \cdot \mathbf{P}_m^c) \cdot \delta \mathbf{x} = \nabla_{0m} \cdot (\mathbf{P}_m^c \cdot \delta \mathbf{x}),$$

and the divergence theorem have been used.

Now it is easy to verify that the three types of boundary conditions: prescribed displacements (3), prescribed tractions (4), or the periodicity conditions (5) and (6) all satisfy the Hill–Mandel condition *a priori*, if the averaging relations for the deformation gradient tensor (7) and for the first Piola–Kirchhoff stress tensor (12) are adopted. In the case of the prescribed displacements (3), substitution of the variation of the boundary position vectors $\delta \mathbf{x} = \delta \mathbf{F}_M \cdot \mathbf{X}$ into the expression for the averaged microwork (18) with incorporation of (14) gives

$$\delta W_{0M} = \frac{1}{V_0} \int_{\Gamma_0} \mathbf{p} \cdot (\delta \mathbf{F}_M \cdot \mathbf{X}) d\Gamma_0 = \frac{1}{V_0} \int_{\Gamma_0} \mathbf{p} \mathbf{X} d\Gamma_0 : \delta \mathbf{F}_M^c = \mathbf{P}_M : \delta \mathbf{F}_M^c. \quad (19)$$

Similarly, substitution of the traction boundary condition (4) into (18), with account for the variation of the macroscopic deformation gradient tensor obtained by varying relation (7), leads to

$$\delta W_{0M} = \frac{1}{V_0} \int_{\Gamma_0} (\mathbf{N} \cdot \mathbf{P}_M^c) \cdot \delta \mathbf{x} d\Gamma_0 = \mathbf{P}_M : \frac{1}{V_0} \int_{\Gamma_0} \mathbf{N} \delta \mathbf{x} d\Gamma_0 = \mathbf{P}_M : \delta \mathbf{F}_M^c. \quad (20)$$

Finally, for the periodic boundary conditions (5) and (6),

$$\begin{aligned} \delta W_{0M} &= \frac{1}{V_0} \left\{ \int_{\Gamma_0^+} \mathbf{p}^+ \cdot \delta \mathbf{x}^+ d\Gamma_0 + \int_{\Gamma_0^-} \mathbf{p}^- \cdot \delta \mathbf{x}^- d\Gamma_0 \right\} \\ &= \frac{1}{V_0} \int_{\Gamma_0^+} \mathbf{p}^+ \cdot (\delta \mathbf{x}^+ - \delta \mathbf{x}^-) d\Gamma_0 \\ &= \frac{1}{V_0} \int_{\Gamma_0} \mathbf{p}^+ (\mathbf{X}^+ - \mathbf{X}^-) d\Gamma_0 : \delta \mathbf{F}_M^c \\ &= \frac{1}{V_0} \int_{\Gamma_0} \mathbf{p} \mathbf{X} d\Gamma_0 : \delta \mathbf{F}_M^c = \mathbf{P}_M : \delta \mathbf{F}_M^c. \end{aligned} \quad (21)$$

5. FE Implementation

5.1. RVE boundary value problem

The RVE problem to be solved is a standard non-linear quasi-static BVP with kinematic boundary conditions.^a Thus, any numerical technique suitable for solution of this type of problems may be used. In the following, the FEM will be adopted. Following the standard FE procedure for the microlevel RVE, after discretisation, the weak form of equilibrium (1) with account for the constitutive relations (2) leads to a system of non-linear algebraic equations in the unknown nodal displacements \mathbf{u} :

$$\mathbf{f}_{\text{int}}(\mathbf{u}) = \mathbf{f}_{\text{ext}}, \quad (22)$$

expressing the balance of internal and external nodal forces. This system has to be completed by boundary conditions. Hence, the earlier introduced boundary conditions (3) or (5) have to be elaborated in more detail.

5.1.1. Fully prescribed boundary displacements

In the case of the fully prescribed displacement boundary conditions (3), the displacements of all nodes on the boundary are simply given by

$$\mathbf{u}_p = (\mathbf{F}_M - \mathbf{I}) \cdot \mathbf{X}_p, \quad p = \overline{1, N_p} \quad (23)$$

where N_p is the number of prescribed nodes, which in this case equals the number of boundary nodes. The boundary conditions (23) are added to the system (22) in a standard manner by static condensation, Lagrange multipliers, or penalty functions.

5.1.2. Periodic boundary conditions

Before application of the periodic boundary conditions (5), they have to be rewritten into a format more suitable for the FE framework. Consider a two-dimensional periodic RVE schematically depicted in Fig. 4. The boundary of this RVE can be split into four parts, here denoted as “T” top, “B” bottom, “R” right and “L” left. For the following it is supposed that the FE discretization is performed such that the distribution of nodes on opposite RVE edges is equal. During the initial periodicity of the RVE, for every respective pair of nodes on the top–bottom and right–left boundaries it is

^aThe traction boundary conditions are not considered in the following, as they do not fit into the deformation-driven procedure, as has been discussed above.

valid in the reference configuration

$$\begin{aligned}\mathbf{X}_T - \mathbf{X}_B &= \mathbf{X}_4 - \mathbf{X}_1, \\ \mathbf{X}_R - \mathbf{X}_L &= \mathbf{X}_2 - \mathbf{X}_1,\end{aligned}\tag{24}$$

where $\mathbf{X}_p, p = 1, 2, 4$ are the position vectors of the corner nodes 1, 2, and 4 in the undeformed state. Then by considering pairs of corresponding nodes on the opposite boundaries, (5) can be written as

$$\begin{aligned}\mathbf{x}_T - \mathbf{x}_B &= \mathbf{F}_M \cdot (\mathbf{X}_4 - \mathbf{X}_1), \\ \mathbf{x}_R - \mathbf{x}_L &= \mathbf{F}_M \cdot (\mathbf{X}_2 - \mathbf{X}_1).\end{aligned}\tag{25}$$

Now if the position vectors of the corner nodes in the deformed state are prescribed according to

$$\mathbf{x}_p = \mathbf{F}_M \cdot \mathbf{X}_p, \quad p = 1, 2, 4\tag{26}$$

then the periodic boundary conditions may be rewritten as

$$\begin{aligned}\mathbf{x}_T &= \mathbf{x}_B + \mathbf{x}_4 - \mathbf{x}_1, \\ \mathbf{x}_R &= \mathbf{x}_L + \mathbf{x}_2 - \mathbf{x}_1.\end{aligned}\tag{27}$$

Since these conditions are trivially satisfied in the undeformed configuration (cf. relation (24)), they may be formulated in terms of displacements

$$\begin{aligned}\mathbf{u}_T &= \mathbf{u}_B + \mathbf{u}_4 - \mathbf{u}_1, \\ \mathbf{u}_R &= \mathbf{u}_L + \mathbf{u}_2 - \mathbf{u}_1,\end{aligned}\tag{28}$$

and

$$\mathbf{u}_p = (\mathbf{F}_M - \mathbf{I}) \cdot \mathbf{X}_p, \quad p = 1, 2, 4.\tag{29}$$

In a discretised format the relations (28) lead to a set of homogeneous constraints of the type

$$\underline{C}_a u_a = 0,\tag{30}$$

where \underline{C}_a is a matrix containing coefficients in the constraint relations and u_a is a column with the degrees of freedom involved in the constraints. Procedures for imposing constraints (30) include the direct elimination of the dependent degrees of freedom from the system of equations, or the use of Lagrange multipliers or penalty functions. In the following, constraints (30) are enforced by elimination of the dependent degrees of freedom. Although such a procedure may be found in many works on finite elements,⁵¹ here it is summarised for the sake of completeness and also in the context of the derivation of the macroscopic tangent stiffness, which will be presented in Sec. 5.3.

First, (30) is partitioned according to

$$\begin{bmatrix} \underline{C}_i & \underline{C}_d \end{bmatrix} \begin{bmatrix} u_i \\ u_d \end{bmatrix} = 0, \quad (31)$$

where u_i are the independent degrees of freedom (to be retained in the system) and u_d are the dependent degrees of freedom (to be eliminated from the system). Because there are as many dependent degrees of freedom u_d as there are independent constraint equations in (31), matrix \underline{C}_d is square and non-singular. Solution for u_d yields

$$u_d = \underline{C}_{di} u_i, \quad \text{with } \underline{C}_{di} = -\underline{C}_d^{-1} \underline{C}_i. \quad (32)$$

This relation may be further rewritten as

$$\begin{bmatrix} u_i \\ u_d \end{bmatrix} = \underline{T} u_i, \quad \text{with } \underline{T} = \begin{bmatrix} \underline{I} \\ \underline{C}_{di} \end{bmatrix}, \quad (33)$$

where \underline{I} is a unit matrix of size $[N_i \times N_i]$, with N_i being the number of independent degrees of freedom.

With the transformation matrix \underline{T} defined such that $\underline{d} = \underline{T} \underline{d}'$, the common transformations $\underline{r}' = \underline{T}^T \underline{r}$ and $\underline{K}' = \underline{T}^T \underline{K} \underline{T}$ can be applied to a linear system of equations of the form $\underline{K} \underline{d} = \underline{r}$, leading to a new system $\underline{K}' \underline{d}' = \underline{r}'$.

The standard linearisation of the non-linear system of equations (22) leads to a linear system in the iterative corrections δu to the current estimate u . This system may be partitioned as

$$\begin{bmatrix} \underline{K}_{ii} & \underline{K}_{id} \\ \underline{K}_{di} & \underline{K}_{dd} \end{bmatrix} \begin{bmatrix} \delta u_i \\ \delta u_d \end{bmatrix} = \begin{bmatrix} \delta r_i \\ \delta r_d \end{bmatrix}, \quad (34)$$

with the residual nodal forces at the right-hand side. Noting that all constraint equations considered above are linear, and thus their linearisation is straightforward, application of the transformation (33) to the system (34) gives

$$[\underline{K}_{ii} + \underline{K}_{id} \underline{C}_{di} + \underline{C}_{di}^T \underline{K}_{di} + \underline{C}_{di}^T \underline{K}_{dd} \underline{C}_{di}] \delta u_i = [\delta r_i + \underline{C}_{di}^T \delta r_d]. \quad (35)$$

Note that the boundary conditions (29) prescribing displacements of the corner nodes have not yet been applied. The column of “independent” degrees of freedom u_i includes the prescribed corner nodes u_p among other nodes. The boundary conditions (29) should be applied to the system (35) in a standard manner.

The condition of antiperiodic tractions (6) will be addressed in Sec. 5.2.2.

5.2. Calculation of the macroscopic stress

After the analysis of a microstructural RVE is completed, the RVE-averaged stresses have to be extracted. The macroscopic stress tensor can be calculated by numerically evaluating the volume integral (12). However, it is computationally more efficient to compute the surface integral (14), which can be further simplified for the case of the periodic boundary conditions.

5.2.1. Fully prescribed boundary displacements

For the case of prescribed displacement boundary conditions, the surface integral (14) simply leads to

$$\mathbf{P}_M = \frac{1}{V_0} \sum_{p=1}^{N_p} \mathbf{f}_p \mathbf{X}_p, \quad (36)$$

where \mathbf{f}_p are the resulting external forces at the boundary nodes; \mathbf{X}_p are the position vectors of these nodes in the undeformed state; and N_p is the number of the nodes on the boundary.

5.2.2. Periodic boundary conditions

In order to simplify the surface integral (14) for the case of periodic boundary conditions, consider all forces acting on the RVE boundary subjected to the boundary conditions according to (28) and (29). At the three prescribed corner nodes, the resulting external forces $\mathbf{f}_p^e, p = 1, 2, 4$ act. Additionally, there are forces involved in every constraint (tying) relation (28). For example, for each constraint relation between pairs of the nodes on the bottom–top boundaries there are a tying force at the node on the bottom boundary \mathbf{p}_B^t , a tying force at the node on the top boundary \mathbf{p}_T^t , and tying forces at the corner nodes 1 and 4, \mathbf{p}_1^{tB} and \mathbf{p}_4^{tB} , respectively. Similarly, there are forces \mathbf{p}_L^t , \mathbf{p}_R^t , \mathbf{p}_1^{tL} and \mathbf{p}_2^{tL} corresponding to the left–right constraints. All these forces are schematically shown in Fig. 5.

Each constraint relation satisfies the condition of zero virtual work; thus,

$$\begin{aligned} \mathbf{p}_B^t \cdot \delta \mathbf{x}_B + \mathbf{p}_T^t \cdot \delta \mathbf{x}_T + \mathbf{p}_1^{tB} \cdot \delta \mathbf{x}_1 + \mathbf{p}_4^{tB} \cdot \delta \mathbf{x}_4 &= 0, \\ \mathbf{p}_L^t \cdot \delta \mathbf{x}_L + \mathbf{p}_R^t \cdot \delta \mathbf{x}_R + \mathbf{p}_1^{tL} \cdot \delta \mathbf{x}_1 + \mathbf{p}_2^{tL} \cdot \delta \mathbf{x}_2 &= 0. \end{aligned} \quad (37)$$

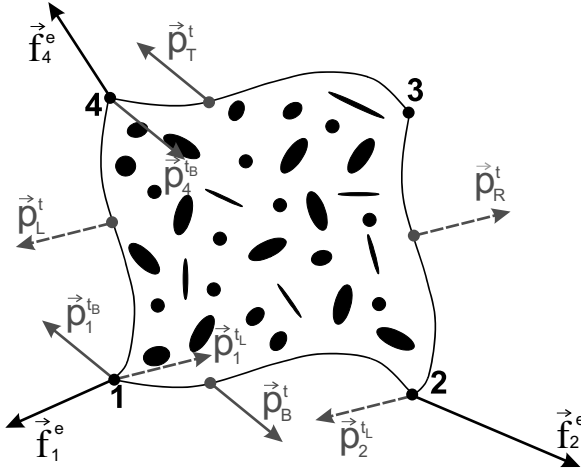


Fig. 5. Schematic representation of the forces acting on the boundary of a two-dimensional RVE subjected to periodic boundary conditions.

Substitution of the variation of the constraints (27) into (37) gives

$$\begin{aligned} (\mathbf{p}_B^t + \mathbf{p}_T^t) \cdot \delta \mathbf{x}_B + (\mathbf{p}_1^{tB} - \mathbf{p}_T^t) \cdot \delta \mathbf{x}_1 + (\mathbf{p}_T^t + \mathbf{p}_4^{tB}) \cdot \delta \mathbf{x}_4 &= 0, \\ (\mathbf{p}_L^t + \mathbf{p}_R^t) \cdot \delta \mathbf{x}_L + (\mathbf{p}_1^{tL} - \mathbf{p}_R^t) \cdot \delta \mathbf{x}_1 + (\mathbf{p}_R^t + \mathbf{p}_2^{tL}) \cdot \delta \mathbf{x}_2 &= 0. \end{aligned} \quad (38)$$

These relations should hold for any $\delta \mathbf{x}_B$, $\delta \mathbf{x}_L$, $\delta \mathbf{x}_1$, $\delta \mathbf{x}_2$, $\delta \mathbf{x}_4$; therefore,

$$\begin{aligned} \mathbf{p}_B^t &= -\mathbf{p}_T^t = -\mathbf{p}_1^{tB} = \mathbf{p}_4^{tB}, \\ \mathbf{p}_L^t &= -\mathbf{p}_R^t = -\mathbf{p}_1^{tL} = \mathbf{p}_2^{tL}. \end{aligned} \quad (39)$$

Note that (39) reflects antiperiodicity of tying forces on the opposite boundaries, thus, the condition (6) is indeed satisfied.

With account for all forces acting on the RVE boundary, the surface integral (14) is written as

$$\begin{aligned} \mathbf{P}_M &= \frac{1}{V_0} \left(\mathbf{f}_1^e \mathbf{X}_1 + \mathbf{f}_2^e \mathbf{X}_2 + \mathbf{f}_4^e \mathbf{X}_4 + \int_{\Gamma_{0B}} \mathbf{p}_B^t \mathbf{X}_B \, d\Gamma_0 + \int_{\Gamma_{0T}} \mathbf{p}_T^t \mathbf{X}_T \, d\Gamma_0 \right. \\ &+ \int_{\Gamma_{0L}} \mathbf{p}_L^t \mathbf{X}_L \, d\Gamma_0 + \int_{\Gamma_{0R}} \mathbf{p}_R^t \mathbf{X}_R \, d\Gamma_0 + \left(\int_{\Gamma_{0B}} \mathbf{p}_1^{tB} \, d\Gamma_0 \right) \mathbf{X}_1 \\ &\left. + \left(\int_{\Gamma_{0L}} \mathbf{p}_1^{tL} \, d\Gamma_0 \right) \mathbf{X}_1 + \left(\int_{\Gamma_{0B}} \mathbf{p}_4^{tB} \, d\Gamma_0 \right) \mathbf{X}_4 + \left(\int_{\Gamma_{0L}} \mathbf{p}_2^{tL} \, d\Gamma_0 \right) \mathbf{X}_2 \right). \end{aligned} \quad (40)$$

Making use of the relation between tying forces (39) gives

$$\begin{aligned} \mathbf{P}_M &= \frac{1}{V_0} \left(\sum_{p=1,2,4} \mathbf{f}_p^e \mathbf{X}_p + \int_{\Gamma_{0B}} \mathbf{p}_B^t (\mathbf{X}_B - \mathbf{X}_T) d\Gamma_0 + \int_{\Gamma_{0L}} \mathbf{p}_L^t (\mathbf{X}_L - \mathbf{X}_R) d\Gamma_0 \right. \\ &\quad + \left(\int_{\Gamma_{0B}} \mathbf{p}_1^{tB} d\Gamma_0 \right) \mathbf{X}_1 + \left(\int_{\Gamma_{0L}} \mathbf{p}_1^{tL} d\Gamma_0 \right) \mathbf{X}_1 \\ &\quad \left. + \left(\int_{\Gamma_{0B}} \mathbf{p}_4^{tB} d\Gamma_0 \right) \mathbf{X}_4 + \left(\int_{\Gamma_{0L}} \mathbf{p}_2^{tL} d\Gamma_0 \right) \mathbf{X}_2 \right). \end{aligned} \quad (41)$$

Inserting the conditions of the initial periodicity of the RVE (24) results in

$$\begin{aligned} \mathbf{P}_M &= \frac{1}{V_0} \left(\sum_{p=1,2,4} \mathbf{f}_p^e \mathbf{X}_p + \int_{\Gamma_{0B}} (\mathbf{p}_B^t + \mathbf{p}_1^{tB}) \mathbf{X}_1 d\Gamma_0 + \int_{\Gamma_{0L}} (\mathbf{p}_L^t + \mathbf{p}_1^{tL}) \mathbf{X}_1 d\Gamma_0 \right. \\ &\quad \left. + \int_{\Gamma_{0B}} (\mathbf{p}_4^{tB} - \mathbf{p}_B^t) \mathbf{X}_4 d\Gamma_0 + \int_{\Gamma_{0L}} (\mathbf{p}_2^{tL} - \mathbf{p}_L^t) \mathbf{X}_2 d\Gamma_0 \right), \end{aligned} \quad (42)$$

which after substitution of the remaining relations between tying forces (39) gives

$$\mathbf{P}_M = \frac{1}{V_0} \sum_{p=1,2,4} \mathbf{f}_p^e \mathbf{X}_p. \quad (43)$$

Therefore, when the periodic boundary conditions are used, all terms with forces involved in the periodicity constraints cancel out from the boundary integral (14) and the only contribution left is by the external forces at the three prescribed corner nodes.

5.3. Macroscopic tangent stiffness

When the micro–macro approach is implemented within the framework of a non-linear FE code, the stiffness matrix at every macroscopic integration point is required. Because in the computational homogenisation approach there is no explicit form of the constitutive behaviour on the macrolevel assumed *a priori*, the stiffness matrix has to be determined numerically from the relation between variations of the macroscopic stress and variations of the macroscopic deformation at such a point. This may be realised by numerical differentiation of the numerical macroscopic stress–strain relation, for example, using a forward difference approximation.⁵² Another approach is to condense the microstructural stiffness to the local macroscopic stiffness. This is achieved by reducing the total RVE

system of equations to the relation between the forces acting on the RVE boundary and the associated boundary displacements. Elaboration of such a procedure in combination with the Lagrange multiplier method to impose boundary constraints can be found in the literature.⁴¹ Here an alternative scheme,^{40,42} which employs the direct condensation of the constrained degrees of freedom, will be considered. After the condensed microscopic stiffness relating the prescribed displacement and force variations is obtained, it needs to be transformed to arrive at an expression relating variations of the macroscopic stress and deformation tensors, typically used in the FE codes. These two steps are elaborated in the following.

5.3.1. Condensation of the microscopic stiffness: Fully prescribed boundary displacements

First the total microstructural system of equations (in its linearised form) is partitioned as

$$\begin{bmatrix} \underline{K}_{pp} & \underline{K}_{pf} \\ \underline{K}_{fp} & \underline{K}_{ff} \end{bmatrix} \begin{bmatrix} \delta \underline{u}_p \\ \delta \underline{u}_f \end{bmatrix} = \begin{bmatrix} \delta \underline{f}_p \\ \underline{0} \end{bmatrix}, \quad (44)$$

where $\delta \underline{u}_p$ and $\delta \underline{f}_p$ are the columns with iterative displacements and external forces of the boundary nodes, respectively; $\delta \underline{u}_f$ is the column with the iterative displacements of the remaining (interior) nodes; and \underline{K}_{pp} , \underline{K}_{pf} , \underline{K}_{fp} and \underline{K}_{ff} are the corresponding partitions of the total RVE stiffness matrix. The stiffness matrix in the formulation (44) is taken at the end of a microstructural increment, where a converged state is reached. Elimination of $\delta \underline{u}_f$ from (44) leads to the reduced stiffness matrix \underline{K}_M relating boundary displacement variations to boundary force variations

$$\underline{K}_M \delta \underline{u}_p = \delta \underline{f}_p \quad \text{with} \quad \underline{K}_M = \underline{K}_{pp} - \underline{K}_{pf} (\underline{K}_{ff})^{-1} \underline{K}_{fp}. \quad (45)$$

5.3.2. Condensation of the microscopic stiffness: Periodic boundary conditions

In the case of the periodic boundary conditions, the point of departure is the microscopic system of equations (35) from which the dependent degrees of freedom have been eliminated (as described in Sec. 5.1.2)

$$\underline{K}^* \delta \underline{u}_i = \delta \underline{r}^*, \quad (46)$$

with

$$\begin{aligned} \underline{K}^* &= \underline{K}_{ii} + \underline{K}_{id} \underline{C}_{di} + \underline{C}_{di}^T \underline{K}_{di} + \underline{C}_{di}^T \underline{K}_{dd} \underline{C}_{di}, \\ \delta \underline{r}^* &= \delta \underline{r}_i + \underline{C}_{di}^T \delta \underline{r}_d. \end{aligned}$$

Next, system (46) is further split, similarly to (44), into the parts corresponding to the variations of the prescribed degrees of freedom δu_p (which in this case are the varied positions of the three corner nodes prescribed according to (29)), variations of the external forces at these prescribed nodes denoted by $\delta \underline{f}_p^*$, and the remaining (free) displacement variations δu_f :

$$\begin{bmatrix} \underline{K}_{pp}^* & \underline{K}_{pf}^* \\ \underline{K}_{fp}^* & \underline{K}_{ff}^* \end{bmatrix} \begin{bmatrix} \delta u_p \\ \delta u_f \end{bmatrix} = \begin{bmatrix} \delta \underline{f}_p^* \\ \underline{0} \end{bmatrix}. \quad (47)$$

Then the reduced stiffness matrix \underline{K}_M^* in the case of periodic boundary conditions is obtained as

$$\underline{K}_M^* \delta u_p = \delta \underline{f}_p^*, \quad \text{with } \underline{K}_M^* = \underline{K}_{pp}^* - \underline{K}_{pf}^* (\underline{K}_{ff}^*)^{-1} \underline{K}_{fp}^*. \quad (48)$$

Note that in the two-dimensional case \underline{K}_M^* is only $[6 \times 6]$ matrix and in three-dimensional case $[12 \times 12]$ matrix.

5.3.3. Macroscopic tangent

Finally, the resulting relation between displacement and force variations (relation (45) if prescribed displacement boundary conditions are used, or relation (48) if periodicity conditions are employed) needs to be transformed to arrive at an expression relating variations of the macroscopic stress and deformation tensors:

$$\delta \mathbf{P}_M = {}^4 \mathbf{C}_M^P : \delta \mathbf{F}_M^c, \quad (49)$$

where the fourth-order tensor ${}^4 \mathbf{C}_M^P$ represents the required consistent tangent stiffness at the macroscopic integration point level.

In order to obtain this constitutive tangent from the reduced stiffness matrix \underline{K}_M^* (or \underline{K}_M^*), first relations (45) and (48) are rewritten in a specific vector/tensor format

$$\sum_j \mathbf{K}_M^{(ij)} \cdot \delta \mathbf{u}_{(j)} = \delta \mathbf{f}_{(i)}, \quad (50)$$

where indices i and j take the values $i, j = \overline{1, N_p}$ for prescribed displacement boundary conditions (N_p is the number of boundary nodes) and $i, j = 1, 2, 4$ for the periodic boundary conditions. In (50) the components of the tensors $\mathbf{K}_M^{(ij)}$ are simply found in the tangent matrix \underline{K}_M^* (for displacement boundary conditions) or in the matrix \underline{K}_M^* (for periodic boundary conditions) at the rows and columns of the degrees of freedom in the nodes i and j .

For example, for the case of the periodic boundary conditions the total matrix $\underline{\mathbf{K}}_{\mathbf{M}}^*$ has the format

$$\underline{\mathbf{K}}_{\mathbf{M}}^* = \begin{bmatrix} \begin{bmatrix} K_{11}^{(11)} & K_{12}^{(11)} \\ K_{21}^{(11)} & K_{22}^{(11)} \end{bmatrix} & \begin{bmatrix} K_{11}^{(12)} & K_{12}^{(12)} \\ K_{21}^{(12)} & K_{22}^{(12)} \end{bmatrix} & \begin{bmatrix} K_{11}^{(14)} & K_{12}^{(14)} \\ K_{21}^{(14)} & K_{22}^{(14)} \end{bmatrix} \\ \begin{bmatrix} K_{11}^{(21)} & K_{12}^{(21)} \\ K_{21}^{(21)} & K_{22}^{(21)} \end{bmatrix} & \begin{bmatrix} K_{11}^{(22)} & K_{12}^{(22)} \\ K_{21}^{(22)} & K_{22}^{(22)} \end{bmatrix} & \begin{bmatrix} K_{11}^{(24)} & K_{12}^{(24)} \\ K_{21}^{(24)} & K_{22}^{(24)} \end{bmatrix} \\ \begin{bmatrix} K_{11}^{(41)} & K_{12}^{(41)} \\ K_{21}^{(41)} & K_{22}^{(41)} \end{bmatrix} & \begin{bmatrix} K_{11}^{(42)} & K_{12}^{(42)} \\ K_{21}^{(42)} & K_{22}^{(42)} \end{bmatrix} & \begin{bmatrix} K_{11}^{(44)} & K_{12}^{(44)} \\ K_{21}^{(44)} & K_{22}^{(44)} \end{bmatrix} \end{bmatrix}, \quad (51)$$

where the superscripts in round brackets refer to the nodes and the subscripts to the degrees of freedom at those nodes. Then each submatrix in (51) may be considered as the representation of a second-order tensor $\mathbf{K}_{\mathbf{M}}^{(ij)}$.

Next, the expression for the variation of the nodal forces (50) is substituted into the relation for the variation of the macroscopic stress following from (36) or (43)

$$\delta \mathbf{P}_{\mathbf{M}} = \frac{1}{V_0} \sum_i \sum_j (\mathbf{K}_{\mathbf{M}}^{(ij)} \cdot \delta \mathbf{u}_{(j)}) \mathbf{X}_{(i)}. \quad (52)$$

Substitution of the equation $\delta \mathbf{u}_{(j)} = \mathbf{X}_{(j)} \cdot \delta \mathbf{F}_{\mathbf{M}}^c$ into (52) gives

$$\delta \mathbf{P}_{\mathbf{M}} = \frac{1}{V_0} \sum_i \sum_j (\mathbf{X}_{(i)} \mathbf{K}_{\mathbf{M}}^{(ij)} \mathbf{X}_{(j)})^{\text{LC}} : \delta \mathbf{F}_{\mathbf{M}}^c, \quad (53)$$

where the superscript LC denotes left conjugation, which for a fourth-order tensor ${}^4\mathbf{T}$ is defined as $T_{ijkl}^{\text{LC}} = T_{jikl}$. Finally, by comparing (53) with (49) the consistent constitutive tangent is identified as

$${}^4\mathbf{C}_{\mathbf{M}}^{\text{P}} = \frac{1}{V_0} \sum_i \sum_j (\mathbf{X}_{(i)} \mathbf{K}_{\mathbf{M}}^{(ij)} \mathbf{X}_{(j)})^{\text{LC}}. \quad (54)$$

If the macroscopic FE scheme requires the constitutive tangent relating the variation of the macroscopic Cauchy stress to the variation of the macroscopic deformation gradient tensor according to

$$\delta \boldsymbol{\sigma}_{\mathbf{M}} = {}^4\mathbf{C}_{\mathbf{M}}^{\sigma} : \delta \mathbf{F}_{\mathbf{M}}^c, \quad (55)$$

this tangent may be obtained by varying the definition equation of the macroscopic Cauchy stress tensor (16), followed by substitution of (36) (or

(43)) and (53). This gives

$$\delta\sigma_{\mathbf{M}} = \left[\frac{1}{V} \sum_i \sum_j (\mathbf{x}_{(i)} \mathbf{K}_{\mathbf{M}}^{(ij)} \mathbf{x}_{(j)})^{\text{LC}} + \frac{1}{V} \sum_i \mathbf{f}_{(i)} \mathbf{I} \mathbf{x}_{(i)} - \sigma_{\mathbf{M}} \mathbf{F}_{\mathbf{M}}^{-c} \right] : \delta \mathbf{F}_{\mathbf{M}}^c, \quad (56)$$

where the expression in square brackets is identified as the required tangent stiffness tensor ${}^4\mathbf{C}_{\mathbf{M}}^\sigma$. In the derivation of (56) it has been used that in the case of prescribed displacements of the RVE boundary (3) or of periodic boundary conditions (5), the initial and current volumes of an RVE are related according to $J_{\mathbf{M}} = \det(\mathbf{F}_{\mathbf{M}}) = V/V_0$.

6. Nested Solution Scheme

Based on the above developments, the actual implementation of the computational homogenisation strategy may be described by the following subsequent steps.

The macroscopic structure to be analysed is discretised by FEs. The external load is applied by an incremental procedure. Increments can be associated with discrete time steps. The solution of the macroscopic non-linear system of equations is performed in a standard iterative manner. To each macroscopic integration point, a discretised RVE is assigned. The geometry of the RVE is based on the microstructural morphology of the material under consideration.

For each macroscopic integration point, the local macroscopic deformation gradient tensor $\mathbf{F}_{\mathbf{M}}$ is computed from the iterative macroscopic nodal displacements (during the initialisation step, zero deformation is assumed throughout the macroscopic structure, i.e. $\mathbf{F}_{\mathbf{M}} = \mathbf{I}$, which allows to obtain the initial macroscopic constitutive tangent). The macroscopic deformation gradient tensor is used to formulate the boundary conditions according to (23) or (28) and (29) to be applied on the corresponding representative cell.

The solution of the RVE BVP employing a fine-scale FE procedure provides the resulting stress and strain distributions in the microstructural cell. Using the resulting forces at the prescribed nodes, the RVE averaged first Piola–Kirchhoff stress tensor $\mathbf{P}_{\mathbf{M}}$ is computed according to (36) or (43) and returned to the macroscopic integration point as a local macroscopic stress. From the global RVE stiffness matrix, the local macroscopic consistent tangent ${}^4\mathbf{C}_{\mathbf{M}}^{\mathbf{P}}$ is obtained according to (54).

When the analysis of all microstructural RVEs is finished, the stress tensor is available at every macroscopic integration point. Thus, the internal macroscopic forces can be calculated. If these forces are in balance with the external load, incremental convergence has been achieved and the next time increment can be evaluated. If there is no convergence, the procedure is continued to achieve an updated estimation of the macroscopic nodal displacements. The macroscopic stiffness matrix is assembled using the constitutive tangents available at every macroscopic integration point from the RVE analysis. The solution of the macroscopic system of equations leads to an updated estimation of the macroscopic displacement field. The solution scheme is summarised in Table 1. It is remarked that the two-level scheme outlined above can be used selectively depending on the macroscopic deformation, e.g. in the elastic domain the macroscopic constitutive tangents do not have to be updated at every macroscopic loading step.

7. Computational Example

As an example, the computational homogenisation approach is applied to pure bending of a rectangular strip under plane strain conditions. Both the length and the height of the sample equal 0.2 m, the thickness is taken 1 m. The macromesh is composed of five quadrilateral eight node plane strain reduced integration elements. The undeformed and deformed geometries of the macromesh are schematically depicted in Fig. 6. At the left side the strip is fixed in axial (horizontal) direction, the displacement in transverse (vertical) direction is left free. At the right side the rotation of the cross section is prescribed. As pure bending is considered the behaviour of the strip is uniform in axial direction and, therefore, a single layer of elements on the macrolevel suffices to simulate the situation.

In this example two heterogeneous microstructures consisting of a homogeneous matrix material with initially 12% and 30% volume fractions of voids are studied. The microstructural cells used in the calculations are presented in Fig. 7. It is worth mentioning that the absolute size of the microstructure is irrelevant for the first-order computational homogenisation analysis (see also discussion in Sec. 9.1).

The matrix material behaviour has been described by a modified elasto-visco-plastic Bodner–Partom model.⁵³ This choice is motivated by the intention to demonstrate that the method is well suited for complex

Table 1. Incremental-iterative nested multiscale solution scheme for the computational homogenisation.

Macro	Micro
1. Initialisation	
<ul style="list-style-type: none"> • initialise the macroscopic model • assign an RVE to every integration point • loop over all integration points 	<p>Initialisation RVE analysis</p> <ul style="list-style-type: none"> • prescribe boundary conditions • assemble the RVE stiffness • calculate the tangent ${}^4\mathbf{C}_M^P$
set $\mathbf{F}_M = \mathbf{I}$	$\xrightarrow{\mathbf{F}_M}$
store the tangent	$\xleftarrow{\text{tangent}}$
<ul style="list-style-type: none"> • end integration point loop 	
2. Next increment	
<ul style="list-style-type: none"> • apply increment of the macro load 	
3. Next iteration	
<ul style="list-style-type: none"> • assemble the macroscopic tangent stiffness • solve the macroscopic system • loop over all integration points 	<p>RVE analysis</p> <ul style="list-style-type: none"> • prescribe boundary conditions • assemble the RVE stiffness • solve the RVE problem • calculate \mathbf{P}_M • calculate the tangent ${}^4\mathbf{C}_M^P$
calculate \mathbf{F}_M	$\xrightarrow{\mathbf{F}_M}$
store \mathbf{P}_M	$\xleftarrow{\mathbf{P}_M}$
store the tangent	$\xleftarrow{\text{tangent}}$
<ul style="list-style-type: none"> • end integration point loop • assemble the macroscopic internal forces 	
4. Check for convergence	
<ul style="list-style-type: none"> • if not converged \Rightarrow step 3 • else \Rightarrow step 2 	

microstructural material behaviour, e.g. non-linear history and strain rate dependent at large strains. The material parameters for annealed aluminum AA 1050 have been used⁵³; elastic parameters: shear modulus $G = 2.6 \times 10^4$ MPa, bulk modulus $K = 7.8 \times 10^4$ MPa and viscosity parameters: $\Gamma_0 = 10^8 \text{ s}^{-2}$, $m = 13.8$, $n = 3.4$, $Z_0 = 81.4$ MPa, $Z_1 = 170$ MPa.

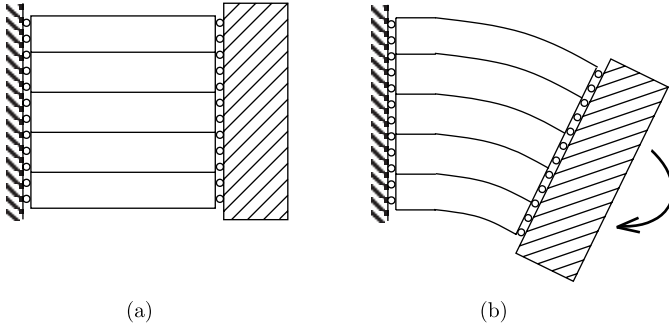


Fig. 6. Schematic representation of the undeformed (a) and deformed (b) configurations of the macroscopically bended specimen.

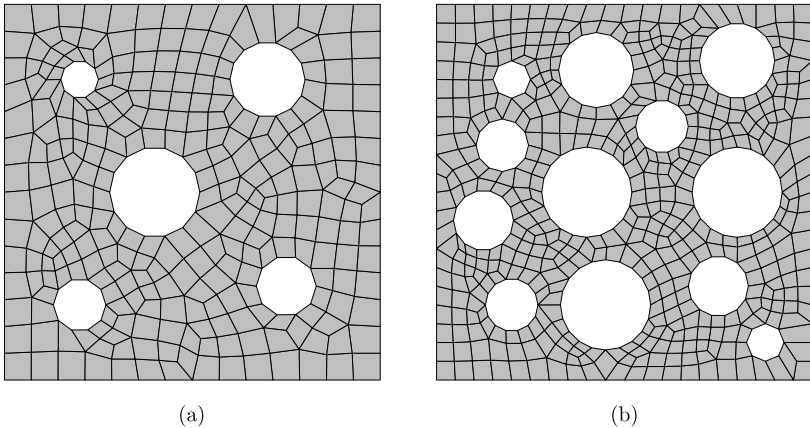


Fig. 7. Microstructural cells used in the calculations with 12% voids (a) and 30% voids (b).

Micro-macro calculations for the heterogeneous structure, represented by the RVEs shown in Fig. 7, have been carried out, simulating pure bending at a prescribed moment rate equal to $5 \times 10^5 \text{ N m s}^{-1}$. Figure 8 shows the distribution plots of the effective plastic strain for the case of the RVE with 12% volume fraction voids at an applied moment equal to $6.8 \times 10^5 \text{ N m}$ in the deformed macrostructure and in three deformed, initially identical RVEs at different locations in the macrostructure. Each hole acts as a plastic strain concentrator and causes higher strains in the RVE than those occurring in the homogenised macrostructure. In the present calculations

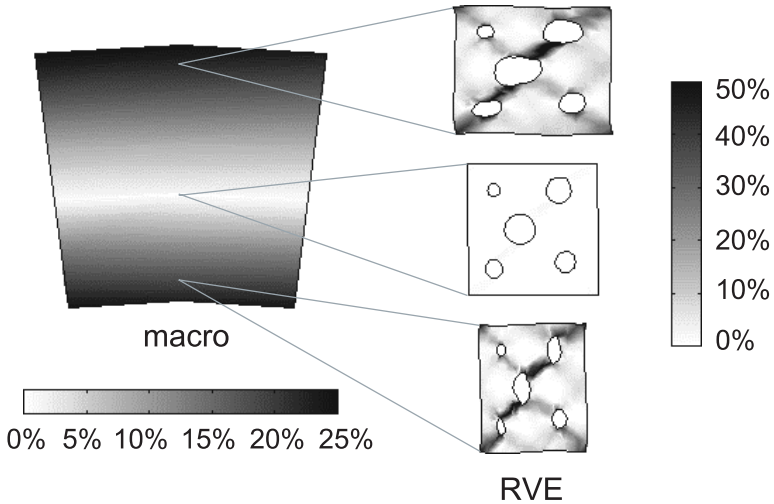


Fig. 8. Distribution of the effective plastic strain in the deformed macrostructure and in three deformed RVEs, corresponding to different points of the macrostructure.

the maximum effective plastic strain in the macrostructure is about 25%, whereas at RVE level this strain reaches 50%. It is obvious from the deformed geometry of the holes in Fig. 8 that the RVE in the upper part of the bended strip is subjected to tension and the RVE in the lower part to compression, while the RVE in the vicinity of the neutral axis is loaded considerably less than the other RVEs. This confirms the conclusion that the method realistically describes the deformation modes of the microstructure.

In Fig. 9, the moment–curvature (curvature defined for the bottom edge of the specimen) diagram resulting from the computational homogenisation approach is presented. To give an impression of the influence of the holes as well, the response of a homogeneous configuration (without cavities) is shown. It can be concluded that even the presence of 12% voids induces a reduction in the bending moment (at a certain curvature) of more than 25% in the plastic regime. This significant reduction in the bending moment may be attributed to the formation of microstructural shear bands, which are clearly observed in Fig. 8. This indicates that in order to capture such an effect a detailed microstructural analysis is required. A straightforward application of, for example, the rule of mixtures would lead to erroneous results.

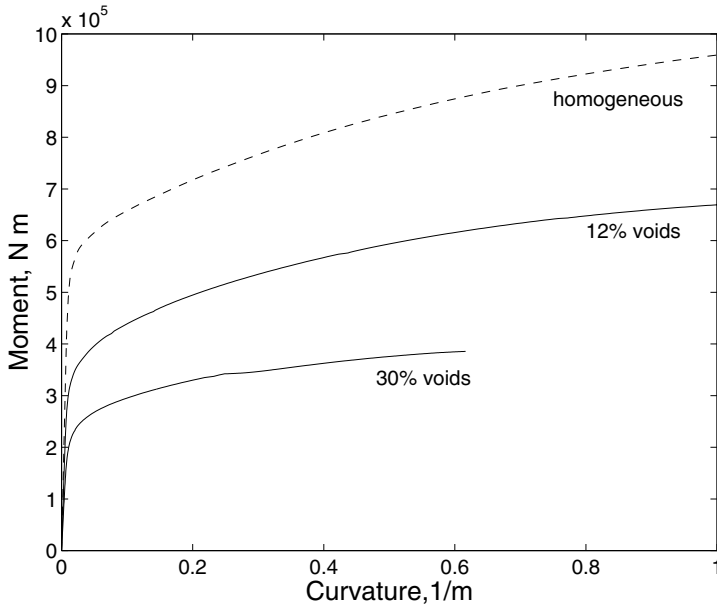


Fig. 9. Moment–curvature diagram resulting from the first-order computational homogenisation analysis.

8. Concept of an RVE within Computational Homogenisation

The computational homogenisation approach, as well as most of other homogenisation techniques, is based on the concept of a representative volume element (RVE). An RVE is a model of a material microstructure to be used to obtain the response of the corresponding homogenised macroscopic continuum in a macroscopic material point. Thus, the proper choice of the RVE largely determines the accuracy of the modelling of a heterogeneous material.

There appear to be two significantly different ways to define an RVE.⁵⁴ The first definition requires an RVE to be a statistically representative sample of the microstructure, i.e. to include virtually a sampling of all possible microstructural configurations that occur in the composite. Clearly, in the case of a non-regular and non-uniform microstructure such a definition leads to a considerably large RVE. Therefore, RVEs that

rigorously satisfy this definition are rarely used in actual homogenisation analyses. This concept is usually employed when a computer model of the microstructure is being constructed based on experimentally obtained statistical information.^{55,56}

Another definition characterises an RVE as the smallest microstructural volume that sufficiently accurately represents the overall macroscopic properties of interest. This usually leads to much smaller RVE sizes than the statistical definition described above. However, in this case the minimum required RVE size also depends on the type of material behaviour (e.g. for elastic behaviour usually much smaller RVEs suffice than for plastic behaviour), macroscopic loading path and contrast in properties between heterogeneities. Moreover, the minimum RVE size, which results in a good approximation of the overall material properties, does not always lead to adequate distributions of the microfields within the RVE. This may be important if, for example, microstructural damage initiation or evolving microstructures are of interest.

The latter definition of an RVE is closely related to the one established by Hill,⁴⁸ who argued that an RVE is well defined if it reflects the material microstructure and if the responses under uniform displacement and traction boundary conditions coincide. If a microstructural cell does not contain sufficient microstructural information, its overall responses under uniform displacement and traction boundary conditions will differ. The homogenised properties determined in this way are called “apparent”, a notion introduced by Huet.⁵⁷ The apparent properties obtained by application of uniform displacement boundary conditions on a microstructural cell usually overestimate the real effective properties, while the uniform traction boundary conditions lead to underestimation. For a given microstructural cell size, the periodic boundary conditions provide a better estimation of the overall properties than the uniform displacement and uniform traction boundary conditions.^{46,47,58,59} This conclusion also holds if the microstructure does not really possess geometrical periodicity. Increasing the size of the microstructural cell leads to a better estimation of the overall properties, and, finally, to a “convergence” of the results obtained with the different boundary conditions to the real effective properties of the composite material, as schematically illustrated in Fig. 10. The convergence of the apparent properties towards the effective ones at increasing size of the microstructural cell has been investigated in by a number of authors.^{47,57–63}

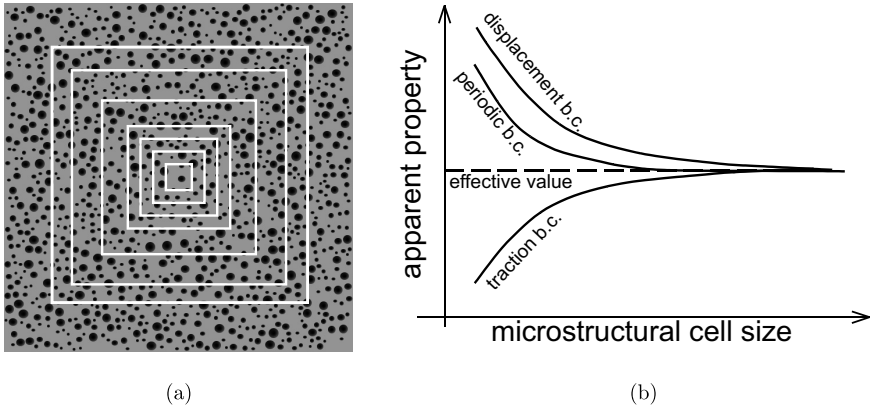


Fig. 10. (a) Several microstructural cells of different sizes. (b) Convergence of the apparent properties to the effective values with increasing microstructural cell size for different types of boundary conditions.

9. Extensions of the Classical Computational Homogenisation Scheme

9.1. Homogenisation towards second gradient continuum

The classical first-order computational homogenisation framework, as presented above, relies on the principle of scale separation, which restricts its applicability limits. The fundamental scale separation concept used in the first-order scheme (and also accepted in most other classical homogenisation approaches) requires that the microstructural length scale is negligible in comparison with the macrostructural characteristic length (determined by the characteristic wave length of the macroscopic load). In this case it is justified to assume macroscopic uniformity of the deformation field over the microstructural RVE. As a result, only simple first-order deformation modes (tension, compression, shear, or combinations thereof) of the microstructure are found. As can be noticed, for example, in Fig. 8, a typical bending mode, which from a physical point of view should appear for small, but finite, microstructural cells in the macroscopically bended specimen, is not retrieved. Moreover, the dimensions of the microstructural heterogeneities do not influence the averaging procedure. Increasing the scale of the entire microstructure then leads to identical results. All of this is not surprising, since the first-order approach is fully in line with standard continuum mechanics concepts, where one of the fundamental points of departure is the

principle of local action. In fact this principle states that material points are local, i.e. are identified with an infinitesimal volume only. This infinitesimal character is exactly represented in the behaviour of the microstructural RVEs, which are considered as macroscopic material points. This implies that the size of the microstructure is considered as irrelevant and hence microstructural and geometrical size effects are not taken into account. Furthermore, it has been demonstrated^{42,64} that if a microstructural RVE exhibits overall softening behaviour (due to geometrical softening or material softening of constituents), the macroscopic solution obtained from the first-order computational homogenisation approach fully localises according to the size of the elements used in the macromesh, i.e. the macroscopic BVP becomes ill-posed leading to a mesh-dependent macroscopic response.

In order to deal with these limitations, the classical (first-order) computational homogenisation has been extended to a so-called second-order computational homogenisation framework,^{42,65,66} which aims at capturing of macroscopic localisation and microstructural size effects. A general scheme of the second-order computational homogenisation approach is shown in Fig. 11 (cf. Fig. 3).

In the second-order homogenisation approach, the macroscopic deformation gradient tensor \mathbf{F}_M and its gradient $\nabla_{0M}\mathbf{F}_M$ are used to formulate boundary conditions for a microstructural RVE. Every microstructural constituent is modelled as a classical continuum, characterised by standard first-order equilibrium and constitutive equations. Therefore, for the

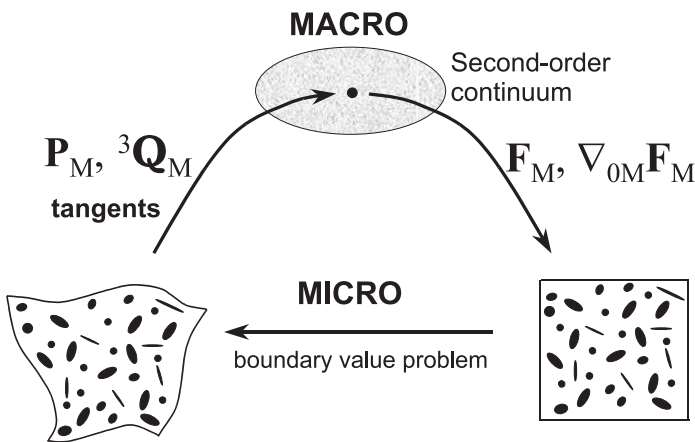


Fig. 11. Second-order computational homogenisation scheme.

description of the microstructural phenomena already available models developed for the first-order homogenisation can be directly employed. On the macrolevel, however, a full second gradient equilibrium problem (of the type originally proposed by Mindlin^{67,68}) appears. From the solution of the underlying microstructural BVP, the macroscopic stress tensor \mathbf{P}_M and a higher-order stress tensor ${}^3\mathbf{Q}_M$ (a third-order tensor, defined as the work conjugate of the gradient of the deformation gradient tensor) are derived based on an extension of the classical Hill–Mandel condition. This automatically delivers the microstructurally based constitutive response of the second gradient macrocontinuum. Consistent (higher-order) tangents of this second-gradient continuum are extracted from the microstructural stiffness using a procedure similar to the one presented for the classical homogenisation. Moreover, it has been shown⁶⁹ that the size of the microstructural RVE used in the second-order computational homogenisation scheme may be related to the length scale of the associated macroscopic homogenised higher-order continuum. Details of the second-order computational homogenisation, its implementation and application examples may be found in the literature.^{42,65,66,69}

9.2. Computational homogenisation for beams and shells

Beam and shell structures have been efficiently and economically applied in various fields of engineering for centuries. Structured and layered thin sheets are used in a variety of innovative applications as well. A typical example is flexible electronics, e.g. flexible displays, where stacks of different materials with complex geometries and interconnects between layers, prohibit the use of classical layer-wise composite shell theory.⁷⁰ For these complex applications, a computational homogenisation technique for thin structured sheets has recently been proposed.^{71,72} In this case the actual three-dimensional heterogeneous sheet is represented by a homogenised shell continuum for which the constitutive response is obtained from the analysis of a microstructural RVE, representing the full thickness of the sheet and an in-plane cell of the macroscopic structure (e.g. a single pixel of a flexible display). The computational homogenisation for structured thin sheets is schematically illustrated in Fig. 12.

Consider a material point of the shell continuum (in-plane integration point in an FE setting). At this macroscopic point generalised strains are assumed to be known. In the particular case of a Mindlin–Reisner shell, these generalised strains are the membrane strain tensor \mathcal{E}_M , the curvature

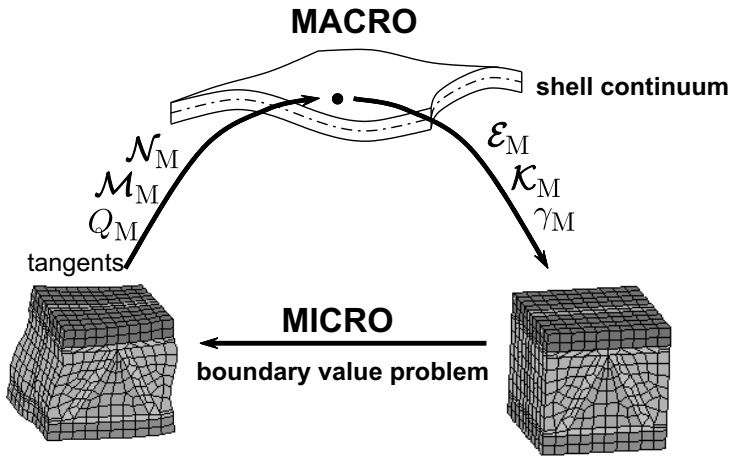


Fig. 12. Scheme of the computational homogenisation for structured thin sheets.

tensor \mathcal{K}_M and the transverse shear strain γ_M . The application of the scheme to other shell formulations (e.g. solid-like shells) can also be developed. The vicinity of this macroscopic point is represented by a microstructural through-thickness RVE. At the RVE scale all microstructural constituents are treated as an ordinary continuum, described by the standard first-order equilibrium and constitutive equations. The microscopic BVP is completed by essential and natural boundary conditions, whereby the macroscopic generalised strains are used to formulate the kinematical boundary conditions on the lateral faces of the RVE, while the top and bottom RVE faces (corresponding to the faces of the macroscopic shell) can be left traction-free (which is typically relevant for shells that are not loaded in the out-of-plane direction, e.g. flexible displays) or other boundary conditions consistent with the out-of-plane loading of the shell can be prescribed.

Upon the solution of the microstructural BVP, the macroscopic generalised stress resultants, i.e. the stress resultant \mathcal{N}_M , the couple-stress resultant (moment) \mathcal{M}_M and the transverse shear resultant Q_M , are obtained by proper averaging the resulting RVE stress field. In this way, the in-plane homogenisation is directly combined with a through-thickness stress integration. Thus, from a macroscopic point of view, a (numerical) generalised stress-strain constitutive response at every macroscopic in-plane integration point is obtained. The macroscopic consistent tangent operators are also extracted through the condensation of the total

microstructural stiffness in a structurally similar manner as discussed above. Additionally, the simultaneously resolved microscale RVE local deformation and stress fields provide valuable information for assessing the reliability of a particular microstructural design. More details on the computational homogenisation for shell structures can be found in the literature.^{71,72}

9.3. Computational homogenisation for heat conduction problems

Materials and structures are often subjected to thermal loading, which may also be transient in nature, e.g. in the case of thermoshock. Typical examples of materials subjected to strong temperature changes and cycles include thermal coatings, refractories in furnaces, microelectronics components and engines. Deterioration and failure of the components at the macroscale is known to originate from non-uniformity and mismatches between microstructural constituents at the microscale resulting in thermal expansion anisotropy and internal stress gradients. A computational homogenisation approach for the coupled multiscale analysis of evolving thermal fields in heterogeneous solids with complex microstructures and including temperature- and orientation-dependent conductivities has recently been proposed by Özdemir *et al.*⁷³ The computational homogenisation framework for heat conduction problems is schematically illustrated in Fig. 13.

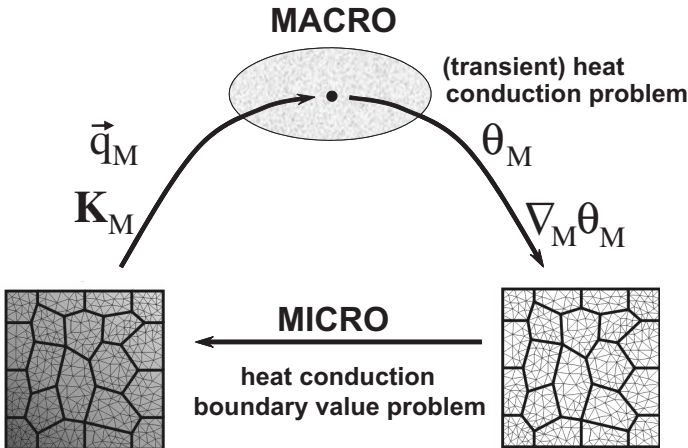


Fig. 13. Scheme of the computational homogenisation for heat conduction problems.

At the macro level, a (transient) heat conduction problem is considered, for which the thermal constitutive behaviour is not formulated explicitly, but which is numerically obtained through a multiscale analysis. At each macroscopic (integration) point, temperature θ_M and temperature gradient $\nabla_M \theta_M$ are calculated and used to define the boundary conditions to be imposed on the microscopic RVE associated with this particular point. The thermal constitutive behaviour of each phase at the micro level is assumed to be known. After solving the microscopic heat conduction BVP, the macroscopic heat flux \bar{q}_M is obtained by volume averaging the resulting heat flux field over the RVE. Additionally, the macroscopic (tangent) conductivity \mathbf{K}_M is extracted from the microstructural conductivity. Although the development of the computational homogenisation framework for the heat conduction problems follows the same philosophy as its mechanical counterpart discussed above, it poses some fundamental differences. More details can be found in the literature.⁷³ Combining the heat conduction and the purely mechanical computational homogenisation schemes, a coupled thermo-mechanical computational homogenisation framework can be established and will be published in forthcoming works.

Acknowledgements

Parts of this research were carried out under projects No. ME97020 and No. MC2.03148 “Multi-scale computational homogenisation” in the framework of the Strategic Research Programme of the Netherlands Institute for Metals Research in the Netherlands.

References

1. J. D. Eshelby, The determination of the field of an ellipsoidal inclusion and related problems, *Proc. R. Soc. Lond A* **241**, 376–396 (1957).
2. Z. Hashin, The elastic moduli of heterogeneous materials, *J. Appl. Mech.* **29**, 143–150 (1962).
3. B. Budiansky, On the elastic moduli of some heterogeneous materials, *J. Mech. Phys. Solids* **13**, 223–227 (1965).
4. T. Mori and K. Tanaka, Average stress in the matrix and average elastic energy of materials with misfitting inclusions, *Acta Metall.* **21**, 571–574 (1973).
5. R. Hill, A self-consistent mechanics of composite materials, *J. Mech. Phys. Solids* **13**, 213–222 (1965).

6. R. M. Christensen and K. H. Lo, Solutions for effective shear properties in three phase sphere and cylinder models, *J. Mech. Phys. Solids* **27**, 315–330 (1979).
7. Z. Hashin and S. Shtrikman, A variational approach to the theory of the elastic behaviour of multiphase materials, *J. Mech. Phys. Solids* **11**, 127–140 (1963).
8. Z. Hashin, Analysis of composite materials. A survey, *J. Appl. Mechanics* **50**, 481–505 (1983).
9. J. R. Willis, Variational and related methods for the overall properties of composites, *Adv. Appl. Mech.* **21**, 1–78 (1981).
10. P. Ponte Castañeda and P. Suquet, Nonlinear composite materials, *Adv. Appl. Mech.* **34**, 171–302 (1998).
11. A. Bensoussan, J.-L. Lionis and G. Papanicolaou, *Asymptotic Analysis for Periodic Structures* (North-Holland, Amsterdam, 1978).
12. E. Sanchez-Palencia, *Non-homogeneous Media and Vibration Theory*, Lecture Notes in Physics, Vol. 127 (Springer-Verlag, Berlin, 1980).
13. A. Tolenado and H. Murakami, A high-order mixture model for periodic particulate composites, *Int. J. Solids Struct.* **23**, 989–1002 (1987).
14. F. Devries, H. Dumontet, G. Duvaut and F. Lene, Homogenization and damage for composite structures, *Int. J. Numer. Meth. Eng.* **27**, 285–298 (1989).
15. J. M. Guedes and N. Kikuchi, Preprocessing and postprocessing for materials based on the homogenization method with adaptive finite element methods, *Comput. Meth. Mech. Eng.* **83**, 143–198 (1990).
16. S. J. Hollister and N. Kikuchi, A comparison of homogenization and standard mechanics analysis for periodic porous composites, *Comput. Mech.* **10**, 73–95 (1992).
17. J. Fish, Q. Yu and K. Shek, Computational damage mechanics for composite materials based on mathematical homogenisation, *Int. J. Numer. Meth. Eng.* **45**, 1657–1679 (1999).
18. S. Nemat-Nasser and M. Hori, *Micromechanics: Overall Properties of Heterogeneous Materials* (Elsevier, Amsterdam, 1993).
19. T. Christman, A. Needleman and S. Suresh, An experimental and numerical study of deformation in metal-ceramic composites, *Acta Metall.* **37**, 3029–3050 (1989).
20. V. Tvergaard, Analysis of tensile properties for whisker-reinforced metal-matrix composites, *Acta Metall. Mater.* **38**, 185–194 (1990).
21. G. Bao, J. W. Hutchinson and R. M. McMeeking, Plastic reinforcement of ductile materials against plastic flow and creep, *Acta Metall. Mater.* **39**, 1871–1882 (1991).
22. J. R. Brockenbrough, S. Suresh and H. A. Wienecke, Deformation of metal-matrix composites with continuous fibers: Geometrical effect of fiber distribution and shape, *Acta Metall. Mater.* **39**, 735–752 (1991).
23. T. Nakamura and S. Suresh, Effect of thermal residual stress and fiber packing on deformation of metal-matrix composites, *Acta Metall. Mater.* **41**, 1665–1681 (1993).

24. P. E. McHugh, R. J. Asaro and C. F. Shin, Computational modeling of metal matrix composite materials — II. Isothermal stress–strain behaviour, *Acta Metall. Mater.* **41**, 1477–1488 (1993).
25. O. van der Sluis, P. J. G. Schreurs and H. E. H. Meijer, Effective properties of a viscoplastic constitutive model obtained by homogenisation, *Mech. Mater.* **31**, 743–759 (1999).
26. O. van der Sluis, Homogenisation of structured elastoviscoplastic solids, PhD thesis, Eindhoven University of Technology, Eindhoven, The Netherlands (2001).
27. S. Suresh, A. Mortensen and A. Needleman (eds.), *Fundamentals of Metal-Matrix Composites* (Butterworth-Heinemann, Boston, 1993).
28. P. E. McHugh, R. J. Asaro and C. F. Shin, Computational modeling of metal matrix composite materials — III. Comparison with phenomenological models, *Acta Metall. Mater.* **41**, 1489–1499 (1993).
29. P. M. Suquet, Local and global aspects in the mathematical theory of plasticity, in *Plasticity Today: Modelling, Methods and Applications*, eds. A. Sawczuk and G. Bianchi (Elsevier Applied Science Publishers, London, 1985), pp. 279–310
30. K. Terada and N. Kikuchi, Nonlinear homogenisation method for practical applications, in *Computational Methods in Micromechanics*, eds. S. Ghosh and M. Ostoja-Starzewski, AMD-Vol. 212/MD-Vol. 62 (ASME, 1995), pp. 1–16.
31. S. Ghosh, K. Lee and S. Moorthy, Multiple scale analysis of heterogeneous elastic structures using homogenisation theory and Voronoi cell finite element method, *Int. J. Solids Struct.* **32**, 27–62 (1995).
32. S. Ghosh, K. Lee and S. Moorthy, Two scale analysis of heterogeneous elastic–plastic materials with asymptotic homogenisation and Voronoi cell finite element model, *Comput. Meth. Appl. Mech. Eng.* **132**, 63–116 (1996).
33. R. J. M. Smit, W. A. M. Brekelmans and H. E. H. Meijer, Prediction of the mechanical behaviour of non-linear heterogeneous systems by multi-level finite element modeling, *Comput. Meth. Appl. Mech. Eng.* **155**, 181–192 (1998).
34. C. Miehe, J. Schröder and J. Schotte, Computational homogenization analysis in finite plasticity. Simulation of texture development in polycrystalline materials, *Comput. Meth. Appl. Mech. Eng.* **171**, 387–418 (1999).
35. C. Miehe, J. Schotte and J. Schröder, Computational micro-macro transitions and overall moduli in the analysis of polycrystals at large strains, *Comput. Mater. Sci.* **16**, 372–382 (1999).
36. J. C. Michel, H. Moulinec and P. Suquet, Effective properties of composite materials with periodic microstructure: a computational approach, *Comput. Meth. Appl. Mech. Eng.* **172**, 109–143 (1999).
37. F. Feyel and J.-L. Chaboche, FE² multiscale approach for modelling the elastoviscoplastic behaviour of long fiber SiC/Ti composite materials, *Comput. Meth. Appl. Mech. Eng.* **183**, 309–330 (2000).
38. K. Terada and N. Kikuchi, A class of general algorithms for multi-scale analysis of heterogeneous media, *Comput. Meth. Appl. Mech. Eng.* **190**, 5427–5464 (2001).

39. S. Ghosh, K. Lee and P. Raghavan, A multi-level computational model for multi-scale damage analysis in composite and porous materials, *Int. J. Solids Struct.* **38**, 2335–2385 (2001).
40. V. Kouznetsova, W. A. M. Brekelmans and F. P. T. Baaijens, An approach to micro–macro modeling of heterogeneous materials, *Comput. Mech.* **27**, 37–48 (2001).
41. C. Miehe and A. Koch, Computational micro-to-macro transition of discretized microstructures undergoing small strain, *Arch. Appl. Mech.* **72**, 300–317 (2002).
42. V. Kouznetsova, Computational homogenization for the multi-scale analysis of multi-phase materials, PhD thesis, Eindhoven University of Technology, Eindhoven, The Netherlands (2002).
43. G. K. Sfantos and M. H. Aliabadi, Multi-scale boundary element modelling of material degradation and fracture, *Comput. Meth. Appl. Mech. Eng.* **196**, 1310–1329 (2007).
44. H. Moulinec and P. Suquet, A numerical method for computing the overall response of non-linear composites with complex microstructure, *Comput. Meth. Appl. Mech. Eng.* **157**, 69–94 (1998).
45. C. Oskay and J. Fish, Eigendeformation-based reduced order homogenization for failure analysis of heterogeneous materials, *Comput. Meth. Appl. Mech. Eng.* **196**, 1216–1243 (2007).
46. O. van der Sluis, P. J. G. Schreurs, W. A. M. Brekelmans and H. E. H. Meijer, Overall behaviour of heterogeneous elastoviscoplastic materials: Effect of microstructural modelling, *Mech. Mater.* **32**, 449–462 (2000).
47. K. Terada, M. Hori, T. Kyoya and N. Kikuchi, Simulation of the multi-scale convergence in computational homogenization approach, *Int. J. Solids Struct.* **37**, 2285–2311 (2000).
48. R. Hill, Elastic properties of reinforced solids: Some theoretical principles, *J. Mech. Phys. Solids.* **11**, 357–372 (1963).
49. R. Hill, On macroscopic effects of heterogeneity in elastoplastic media at finite strain, *Math. Proc. Cam. Phil. Soc.* **95**, 481–494 (1984).
50. S. Nemat-Nasser, Averaging theorems in finite deformation plasticity, *Mech. Mater.* **31**, 493–523 (1999).
51. R. D. Cook, D. S. Malkus and M. E. Plesha, *Concepts and Applications of Finite Element Analysis* (Wiley, Chichester, 1989).
52. C. Miehe, Numerical computation of algorithmic (consistent) tangent moduli in large-strain computational inelasticity, *Comput. Meth. Appl. Mech. Eng.* **134**, 223–240 (1996).
53. H. C. E. van der Aa, M. A. H. van der Aa, P. J. G. Schreurs, F. P. T. Baaijens and W. J. van Veenen, An experimental and numerical study of the wall ironing process of polymer coated sheet metal, *Mech. Mater.* **32**, 423–443 (2000).
54. W. J. Drugan and J. R. Willis, A micromechanics-based nonlocal constitutive equation and estimates of representative volume element size for elastic composites, *J. Mech. Phys. Solids* **44**(4), 497–524 (1996).

55. J. Zeman and M. Šejnoha, Numerical evaluation of effective elastic properties of graphite fiber tow impregnated by polymer matrix, *J. Mech. Phys. Solids* **49**, 69–90 (2001).
56. Z. Shan and A. M. Gokhale, Representative volume element for non-uniform micro-structure, *Comput. Mater. Sci.* **24**, 361–379 (2002).
57. C. Huet, Application of variational concepts to size effects in elastic heterogeneous bodies, *J. Mech. Phys. Solids* **38**(6), 813–841 (1990).
58. T. Kanit, S. Forest, I. Galliet, V. Mounoury and D. Jeulin, Determination of the size of the representative volume element for random composites: Statistical and numerical approach, *Int. J. Solids Struct.* **40**, 3647–3679 (2003).
59. T. Kanit, F. N’Guyen, S. Forest, D. Jeulin, M. Reed and S. Singleton, Apparent and effective physical properties of heterogeneous materials: Representativity of samples of two materials from food industry, *Comput. Meth. Appl. Mech. Eng.* **195**, 3960–3982 (2006).
60. C. Huet, Coupled size and boundary-condition effects in viscoelastic heterogeneous and composite bodies, *Mech. Mater.* **31**, 787–829 (1999).
61. M. Ostoja-Starzewski, Random field models of heterogeneous materials, *Int. J. Solids Struct.* **35**(19), 2429–2455 (1998).
62. M. Ostoja-Starzewski, Scale effects in materials with random distributions of needles and cracks, *Mech. Mater.* **31**, 883–893 (1999).
63. S. Pecullan, L. V. Gibiansky and S. Torquato, Scale effects on the elastic behavior of periodic and hierarchical two-dimensional composites, *J. Mech. Phys. Solids* **47**, 1509–1542 (1999).
64. M. G. D. Geers, V. G. Kouznetsova and W. A. M. Brekelmans, Multi-scale first-order and second-order computational homogenisation of microstructures towards continua, *Int. J. Multiscale Comput. Eng.* **1**, 371–386 (2003).
65. V. Kouznetsova, M. G. D. Geers and W. A. M. Brekelmans, Multi-scale constitutive modelling of heterogeneous materials with a gradient-enhanced computational homogenisation scheme, *Int. J. Numer. Meth. Eng.* **54**, 1235–1260 (2002).
66. V. G. Kouznetsova, M. G. D. Geers and W. A. M. Brekelmans, Multi-scale second-order computational homogenization of multi-phase materials: A nested finite element solution strategy, *Comput. Meth. Appl. Mech. Eng.* **193**, 5525–5550 (2004).
67. R. D. Mindlin, Second gradient of strain and surface-tension in linear elasticity, *Int. J. Solids Struct.* **1**, 417–438 (1965).
68. R. D. Mindlin and N. N. Eshel, On first strain-gradient theories in linear elasticity, *Int. J. Solids Struct.* **4**, 109–124 (1968).
69. V. G. Kouznetsova, M. G. D. Geers and W. A. M. Brekelmans, Size of a representative volume element in a second-order computational homogenization framework, *Int. J. Multiscale Comput. Eng.* **2**, 575–598 (2004).
70. J. Hohe and W. Becker, Effective stress–strain relations for two dimensional cellular sandwich cores: Homogenization, material models, and properties, *Appl. Mech. Rev.* **55**, 61–87 (2002).

71. M. G. D. Geers, E. W. C. Coenen and V. G. Kouznetsova, Multi-scale computational homogenisation of structured thin sheets, *Modelling Simul. Mater. Sci. Eng.* **15**, S393–S404 (2007).
72. E. W. C. Coenen, V. G. Kouznetsova and M. G. D. Geers, Computational homogenization for heterogeneous thin sheets, in preparation (2007).
73. I. Özdemir, W. A. M. Brekelmans and M. G. D. Geers, Computational homogenization for heat conduction in heterogeneous solids, *Int. J. Numer. Meth. Eng.* **73**(2), 185–204 (2008).